

A CATALOG OF STELLAR UNIFIED PROPERTIES (CATSUP) FOR 951 FGK-STARS WITHIN 30 PC

NATALIE R. HINKEL¹, ERIC E. MAMAJEK^{2,3}, MARGARET C. TURNBULL⁴, ELLA OSBY⁵, EVGENYA L. SHKOLNIK⁵, GRAEME H. SMITH⁶, ALEXIS KLIMASEWSKI³, GARRETT SOMERS¹, STEVEN J. DESCH⁵

Draft version September 15, 2017

ABSTRACT

Almost every star in our Galaxy is likely to harbor a terrestrial planet, but accurate measurements of an exoplanet’s mass and radius demands accurate knowledge of the properties of its host star. The imminent TESS and CHEOPS missions are slated to discover thousands of new exoplanets. Along with WFIRST, which will directly image nearby planets, these surveys make urgent the need to better characterize stars in the nearby solar neighborhood (< 30 pc). We have compiled the CATALOG of Stellar Unified Properties (CATSUP) for 951 stars, including such data as: Gaia astrometry; multiplicity within stellar systems; stellar elemental abundance measurements; standardized spectral types; Ca II H and K stellar activity indices; GALEX NUV and FUV photometry; and X-ray fluxes and luminosities from ROSAT, XMM, and Chandra. We use this data-rich catalog to find correlations, especially between stellar emission indices, colors, and galactic velocity. Additionally, we demonstrate that thick-disk stars in the sample are generally older, have lower activity, and have higher velocities normal to the galactic plane. We anticipate CATSUP will be useful in discerning other trends among stars within the nearby solar neighborhood, for comparing thin-disk vs. thick-disk stars, for comparing stars with and without planets, and for finding correlations between chemical and kinematic properties.

Subject headings: solar neighborhood — stars: fundamental parameters — catalogs

1. INTRODUCTION

The acceleration of exoplanet detections has shifted the field from one of discovery to one of characterization. Surveys are rapidly becoming complete with respect to Jupiter-sized planets: occurrence rates of gaseous giant planets with masses $> 50 M_{\oplus}$ and periods < 10 years is $\sim 14\%$ (Mayor et al. 2011). Even the discovery of Earth- to super Earth-sized (radii $0.5 - 4 R_{\oplus}$) planets is becoming routine, with an occurrence rate ~ 1 per small star inferred (Dressing & Charbonneau 2013, and references therein). The *Kepler* mission has established that planets are nearly ubiquitous around stars, and even multi-planet systems are common (Batalha et al. 2013). *Kepler* has discovered about 550 rocky exoplanets, including 9 that orbit in their stars’ habitable zones (*Kepler* press release May 10, 2016). Scientific progress in the field of exoplanets has advanced so much, it is possible to go beyond asking where the planets are, to asking what they are made of, a necessary first step to assessing habitability. Finding and characterizing exoplanets are the goals of future space mission such as the Transiting Exoplanet Survey Satellite (TESS), the CHaracterizing ExOPlanets Satellite (CHEOPS), the PLANetary Transits and Oscillations of stars (PLATO) mission, and the Wide-Field InfraRed Survey Telescope (WFIRST).

Electronic address: natalie.hinkel@gmail.com

¹ Department of Physics & Astronomy, Vanderbilt University, Nashville, TN 37235, USA

² Jet Propulsion Laboratory, California Institute of Technology, M/S 321-100, 4800 Oak Grove Drive, Pasadena, CA 91109, USA

³ Department of Physics and Astronomy, University of Rochester, Rochester, NY 14627-0171, USA

⁴ Global Science Institute, P.O. Box 252, Antigo, WI 54409, USA

⁵ School of Earth & Space Exploration, Arizona State University, Tempe, AZ 85287, USA

⁶ University of California Observatories and Department of Astronomy & Astrophysics, University of California, Santa Cruz CA 95064

It is a truism in the exoplanet community that to know the planet one must know the star. Detection of exoplanets has always depended on good characterization of the star. This was true of 51 Pegasi (Gray 1997), to the recent case of HD 219134h, where a planet inferred by Vogt et al. (2015) has been found to have a period equal to the star’s rotation period, making it an artifact of stellar activity (Johnson et al. 2016). To meaningfully constrain exoplanet compositions, one needs to distinguish a bulk density of 2 g cm^{-3} (like the densities of Ganymede and Titan, made of rock and ice per Showman & Malhotra 1999) from one of 5 g cm^{-3} (like the densities of Mercury, Venus, and Earth, with metal cores and rocky mantles per Wanke 1981). To measure density at this precision requires constraining planetary mass and radius, and therefore stellar mass and radius, to within about 10% (Unterborn et al. 2016). In order to move beyond simple questions of whether a planet is rock with ice or rock with a large metal core, inclusion of elemental ratios, inferred from the host star, must be included. The habitability of the planet, and the detectability of life through atmospheric gases, depend on the state of the atmosphere, which is sensitive to high-energy (X-ray and ultraviolet [UV]) emission from the star. At every step, characterization of an exoplanet requires comprehensive information about the host star.

A wealth of information currently exists for the Sun-like (main-sequence, FGK-type) stars within 30 pc that will be the highest priorities for exoplanet searches and observations. We examine stars within a radius 30pc to ensure a certain quality sample of stars that is “complete” for the targets of highest priority direct imaging missions (early/mid-KV and brighter stars, $V > 7-8$ at the faintest). Beyond that distance, there is a decreased ability to detect stellar companions, which results in plummeting quality at the cost of exponentially more work in

vetting the data from other sources on fainter and more distant stars. Yet, despite the availability of useful repositories such as VizieR (Ochsenbein et al. 2000), PASTEL (Soubiran et al. 2016), and TOPCAT (Taylor 2005), no single database contains all the disparate physical and chemical information needed to thoroughly characterize nearby Sun-like stars. What information exists is often spread across several non-standardized databases.

In response, we have created a CAtalog of Stellar Unified Properties (CATSUP) where we combine important stellar information with the goal of expediting characterization of planetary systems, their interior structure, and overall habitability. CATSUP incorporates available stellar information relating to astrometry, multiplicity, stellar activity, and stellar abundances with new, unpublished, high-energy emission data. Specifically, we have included new far-UV (FUV) and near-UV (NUV) emission data from Galaxy Evolution Explorer (GALEX). We have also added X-ray data from the ROSAT, XMM, and Chandra missions that have been combined using a new methodology and put on a uniform baseline. Both UV and X-ray information is important when characterizing a planetary system and for understanding exoplanet atmospheres and their possible evaporation. The number of stars and breadth of data within CATSUP allows access to data that was previously difficult or inaccessible. Even when specific stars aren't listed in the database, data can be cross-correlated in order to form a benchmark from which proxies can be determined based on similar, nearby stars. While we have chosen not to focus specifically on planetary properties within CATSUP, the information for solar neighborhood stars can be utilized to better characterize planets and their host stars. We particularly focus on collating data to assess planetary habitability, to help narrow the observational field, and to optimize the search for Earth-like planets, a particularly important goal as telescope time for follow-up observations is limited.

In this paper we discuss the creation and contents of CATSUP, a catalog of 951 nearby (< 30 pc) FGK main-sequence stars containing an array of datasets relevant to exoplanet detection and characterization. For data already available in the literature, we will briefly summarize the details in an effort to maintain a holistic view of the CATSUP database. We begin with the high-precision astrometric measurements by the Gaia mission (Gaia Collaboration et al. 2016) as the basis for the catalog (Section 2). We include currently available data on system multiplicity from ExoCat (Turnbull 2015, see Section 3), stellar abundance measurements from the Hypatia catalog (Hinkel et al. 2014, see Section 4), collated spectral types (Section 5), and Ca II H and K stellar activity indices (Smith 2011, Section 6). We present UV emission data from GALEX archives (Section 7). Finally, we present X-ray data from the ROSAT, XMM and Chandra missions (Section 8). As an example of the capabilities of the combined database, we present in Section 9 an exploration of the correlation between Ca II H and K indices with color, galactic velocity, and thin-disk vs. thick-disk membership.

2. GAIA

The Tycho-Gaia Astrometric Solution (TGAS, Gaia Collaboration et al. 2016) subset of the Gaia

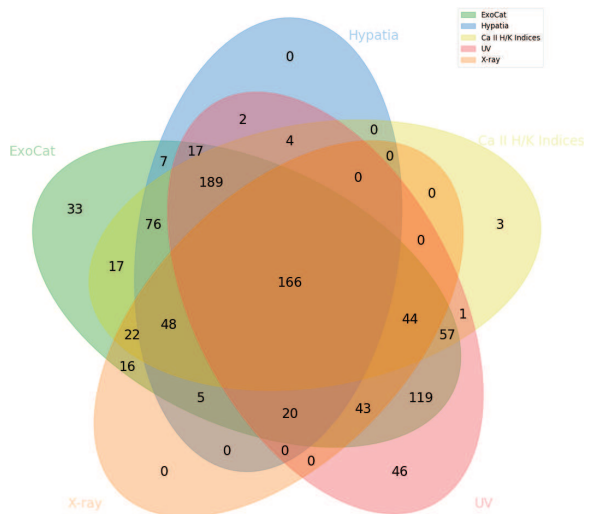


FIG. 1.— A Venn Diagram showing the stars that overlap between datasets within CATSUP, such that 166 stars have measurements from all five sources. The total number, or the sum of all the entries, is 951 FGK-type stars within 30 pc. There are 879 stars in ExoCat, 534 in Hypatia, 627 with the Ca II H and K indices, 708 with GALEX UV data, and 364 with X-ray data. Note: All stars are found within Gaia by design. A total of 48 CATSUP stars, or 5% of the total sample, are currently known to host exoplanets (see Table 6).

survey provides a convenient and logical starting sample for which data important to both stellar and exoplanet scientific studies can be compiled. Despite the fact that TGAS is $\sim 80\%$ complete in reference to both HIPPARCOS and *Tycho-2* (Arenou et al. 2017), the high precision astrometry are valuable for target characterization. Additionally, one of the main reasons for TGAS incompleteness is due to a cut on stars with high parallax errors, namely > 1 mas (Arenou et al. 2017), which is acceptable, if not preferable, given our intention. Therefore, we started by querying TGAS sources available through VizieR⁷ (Ochsenbein et al. 2000). We then placed a 30 pc cutoff, or parallax > 33.33 mas, on the TGAS stars so that we could focus on nearby stars that have both physical and chemical measurements. Note, the distance provided was calculated as the inverse of the parallax, which is a safe assumption for nearby stars as in this case, e.g. Astraatmadja & Bailer-Jones (2016).. Then, using the MK classification of Skiff (see Section 5), we included only FGK-type stars in order to maximize completeness. In this way, CATSUP is able to better achieve catalog completeness by including only nearby main sequence stars with accurate astrometric solutions (Arenou et al. 2017).

The total number of stars with compiled data within CATSUP is 951, shown in Figure 1. By summing each of the separate ellipses, you will get the total number of stars in each dataset: 879 stars in ExoCat, 534 in Hypatia, 627 with the Ca II H and K indices, 708 with GALEX UV data, and 364 with X-ray data. Further-

⁷ <http://vizier.u-strasbg.fr/viz-bin/VizieR-3?-source=I/337/tgas>

more, we have included a flag within Table 6 to indicate whether a star is known to host an exoplanet at the time of this publication, based on the NASA Exoplanet Archive⁸ A summary of the parameters available in CATSUP are given in Table 6 – the full table will be provided via the online journal and through Vizier. In the next sections, we describe the compilation of essential stellar data within CATSUP.

3. EXOCAT

The Nearby Stellar Systems Catalog for Exoplanet Imaging Missions (a.k.a. “ExoCat,” Turnbull 2015) was created for the purpose of supporting the development of exoplanet direct imaging missions such as WFIRST, Exo-S, Hab-Ex, and other concepts (Spergel et al. 2013, 2015; Seager et al. 2015; Mennesson et al. 2016, respectively). The current version of ExoCat contains 2351 entries for Hipparcos stars within 30pc of the Sun. ExoCat provides basic observational data (e.g., Hipparcos astrometry including Equatorial and Galactic coordinates, parallax, and proper motions, Johnson B and V magnitudes, and Ks-band magnitudes from 2MASS or converted to 2MASS Ks magnitudes for bright stars). Using these data, ExoCat contains derived estimates of stellar luminosity, effective temperature, stellar radius and angular size, stellar mass, habitable zone locations and angular size, photometric fractional planet brightness and V-band magnitude for an exo-Earth at the Earth-equivalent insolation distance (see Turnbull 2015, for details). For bright stars ($V < 7$), ExoCat provides separations and delta-magnitudes for the brightest stellar companion within 10 arcseconds, taken from the Washington Double Star catalog (Mason et al. 2001).

All of these star and system parameters are crucial to understanding the necessary performance of an exoplanet imaging mission: from controlling stray light from off-axis companions, to setting requirements on contrast and speckle stability, inner and outer working angles, and throughput, to creating a design reference mission and observing schedule that can be executed within solar avoidance and other engineering constraints. ExoCat is under continuous development in order to provide more accurate system parameters. ExoCat-v1 can be downloaded from the Exoplanets Exploration Program (ExEP) website⁹. There are 879 ExoCat stars within CATSUP, where 878 of those stars can also be found in the TESS Input Catalog (Stassun et al. 2017). Note the TESS Input Catalog was the only target selection list available out of the three upcoming exoplanet missions (TESS, CHEOPS, and WFIRST).

One especially important and complicated piece of information involves binary and multiple systems. ExoCat contains a growing set of system descriptions identifying components that may not be included in Hipparcos (or for which the Hipparcos identifier refers to more than one star); these indicators have been included in CATSUP (see Table 6). Each star is noted as either (a) a true single star per a deep literature source (Table 6, Single = 1), or (b) if known to be a member of a multiple, which component that HIP number is referring to (Table 6,

Component = A, B, etc). In many cases, the HIP number includes more than one star, either a known or suspected unresolved/very faint companion, which is noted by a “+” symbol. In a few cases, the “+” has its own additional entry. If more than one star in the system has its own HIP number, the other associated HIP numbers are listed in the “HIP2” column. As noted in the original ExoCat paper (Turnbull 2015), if the “Single” column does not equal 1 or if there is a “+,” then it is possible that the system does not correspond to only one star. Namely, it is possible that the HIP entry corresponds to more than one object. If that system comes up as a high priority for a future mission, it should be scrutinized more carefully. Of the stars in our catalog with either known single or binary status, $\sim 45\%$ reside in binary or triple systems. This multiplicity fraction matches expectations from volume limited companion surveys, which generally find that 45-50% of main sequence stars in the mass range $0.7\text{-}1.3 M_{\odot}$ (a close match for the CATSUP catalog) are multiples. As a secondary check, we cross reference CATSUP with the Tycho Double Star Catalog (Fabricius et al. 2002), finding that among stars in both catalogs, 49% have companions. We conclude that the binary fraction of our sample is consistent with expectations.

4. THE HYPATIA CATALOG 2.1

The Hypatia Catalog is a composite stellar abundance catalog that is comprised of multiple literature sources of high resolution spectroscopic data (Hinkel et al. 2014, 2016). Since the last update published in Hinkel et al. (2016), we have included 55 additional catalogs from the literature as well as 11 new elements and species (namely: Si II, Nb II, Pr II, Gd II, Tb II, Dy II, Er II, Tm II, Yb II, Hf II, Th II), as shown in Fig. 2. A breakdown of the added data sets, including information regarding the telescopes, models, and techniques, is given in Table 2-5. There are currently 64 elements and species measured in 5986 main-sequence stars within 150 pc of the Sun. Keeping with our naming scheme, we have increased the tenths value of the version number in order to indicate the addition of new data sets.

In addition to the data sets, we have included a number of new stellar properties within Hypatia and updated the source for some of the existing properties. Namely, we now take advantage of the high-precision RAs, Decs, and parallaxes from Gaia, where applicable, or for $\sim 68\%$ of the Hypatia Catalog. For the remaining 32%, we continue our use of Anderson & Francis (2012) for the RAs, Decs, and parallaxes not available in Gaia. Stellar effective temperature (T_{eff}) and surface gravity ($\log(g)$) have been pulled from the PASTEL catalogue (Soubiran et al. 2016), in addition to preferentially using their B and V magnitudes where possible. Finally, Hypatia now incorporates the 2MASS identifier. All properties and original sources of reference are listed in Table 6.

The full Hypatia Catalog Database, including stellar abundances from all individual catalogs, a variety solar normalizations, stellar properties, and planetary properties (where available), can be found at www.hypatiacatalog.com. Multiple interactive plotting interfaces, in addition to tabular data, can be freely accessed through the website to quickly and easily analyze stellar abundance data, including updated version

⁸ exoplanetarchive.ipac.caltech.edu. We found that 48 stars within CATSUP are currently known to host exoplanets.

⁹ <http://nexsci.caltech.edu/missions/EXEP/EXEPstarlist.html>

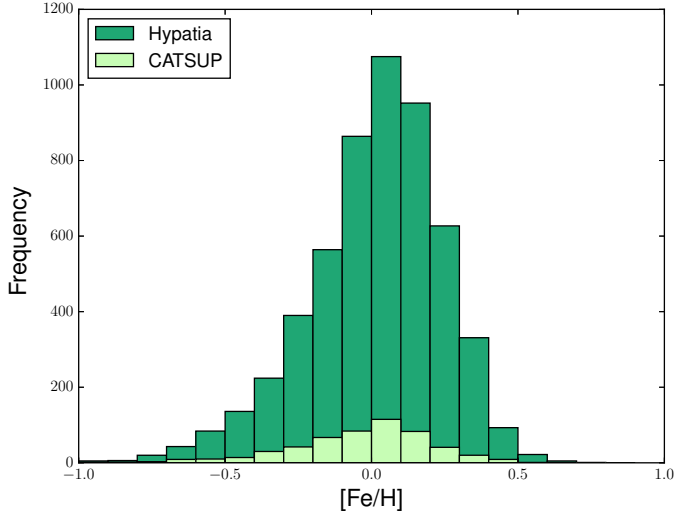


FIG. 3.— Frequency distribution showing the number of stars in Hypatia (dark green) and CATSUP (light green) with respect to $[\text{Fe}/\text{H}]$. The x-axis is binned in 0.1 dex per the typical error associated with $[\text{Fe}/\text{H}] = \pm 0.05$ dex.

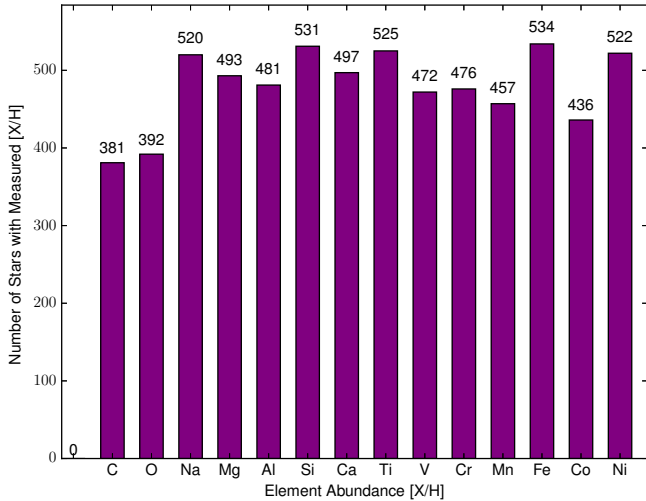


FIG. 4.— Similar to Fig. 2, here we show the number of stars in CATSUP that have measurements for each element along the x-axis. The total number of stars in both CATSUP and Hypatia is 534.

liarities, binarity, etc.). There were minor shifts in the spectral types of some FGK-standard stars between the 1940s and 1980s by Philip C. Keenan. In the interest to have the spectral types as close to being on the modern MK system as possible (represented by the dwarf standards of Keenan & McNeil 1989 among the FGK-type stars), we preferentially adopted spectral types classified since 1989, and especially those published by expert classifiers using CCD spectra (e.g. Gray et al. 2003, 2006).

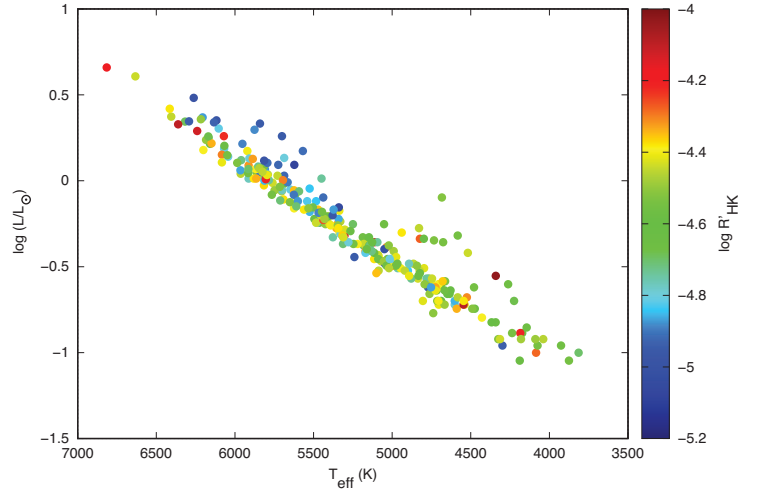


FIG. 5.— Hertzsprung-Russell diagram of 270 CATSUP stars, where stars are color coded according to $\log R'_{\text{HK}}$ emission measurements of stellar activity. This figure was made using Filtergraph (Burger et al. 2013).

Classifications from the Michigan Spectral Survey (e.g. Houk & Cowley 1975) are only used where necessary, as their standard star grid varied somewhat from modern grids. This variation results in systematic offsets sometimes at the ± 1.5 subtype level, however these can be corrected following Table 5 of the Pecaut & Mamajek (2016) paper. A total of 6 spectral types for the CATSUP stars were adjusted from the Michigan Spectral Survey and have been annotated with an asterisk next to their reference in Table 6. For some subtypes (e.g. K3V), no adjustment was necessary. Fortunately, most nearby bright stars in our survey had CCD spectra classified by the NStars project by Gray et al. (2003) and Gray et al. (2006), based on the modern grid of standards discussed in §4.1 of Pecaut & Mamajek (2016). The spectral types for the CATSUP stars, and their respective sources, can be found in Table 6.

6. CA II H AND K INDICES

A widely utilized measure of stellar activity derivable from ground-based observations has been the amount of chromospheric emission in the cores of the Ca II H and K lines, at 3968 Å and 3933 Å, respectively. One of the most physically meaningful parameterizations of this emission is the R'_{HK} index that is defined by Noyes et al. (1984) as being the chromospheric flux in the combined H and K lines radiated by a star relative to the bolometric flux of the star. It is an index that has been corrected for photospheric contributions to the flux across the wavelengths of the H₂ and K₂ lines, which are the chromospheric emission (reversals) of the Ca II H and K lines. Early discussions of the behavior of this index, or similar ones not corrected for a photospheric component, among nearby late-type dwarf stars can be found in Middelkoop (1982); Hartmann et al. (1984); Noyes et al. (1984); Soderblom (1985), all of whom built on the work

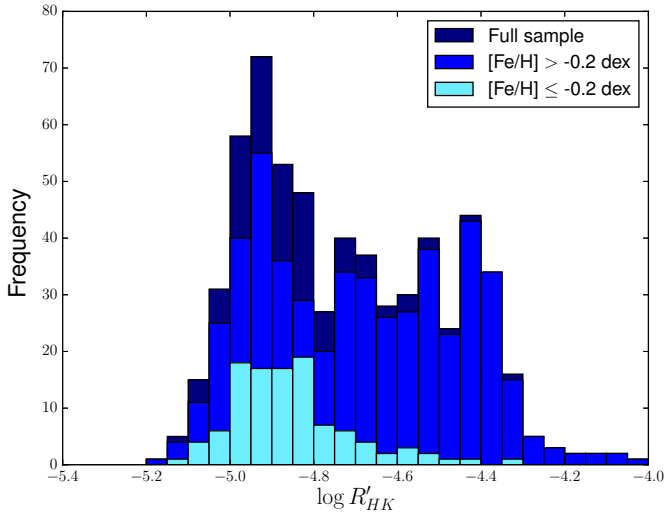


FIG. 6.— Frequency distribution of the CATSUP stars with respect to $\log R'_{HK}$ for two populations of stars, one with $[\text{Fe}/\text{H}] > -0.2$ dex and one with $[\text{Fe}/\text{H}] < -0.2$ dex. Both distributions are shown with 0.05 bins of $\log R'_{HK}$ in keeping with Henry et al. (1996); Gray et al. (2006); Jenkins et al. (2011).

of Wilson (1978); Vaughan & Preston (1980).

Values of $\log R'_{HK}$ emission measurements, are listed in Table 6, for 627 stars within CATSUP, Table 6. These values were selected from a larger data base that were compiled from papers in the literature prior to 2011 per (Smith 2011), in addition to two stars from Gomes da Silva et al. (2014). The characteristics of this pre-2011 data base of $\log R'_{HK}$ values have been discussed by Smith & Redenbaugh (2010) and Smith (2011), who also describe the manner in which the data base was compiled. By far the largest literature sources used in the compilation of Smith (2011) are the following: Gray et al. (2003, 2006); Henry et al. (1996); Jenkins et al. (2006, 2008); Noyes et al. (1984); Soderblom (1985); Soderblom et al. (1991); Wright et al. (2004). Where multiple literature values were available they were averaged with equal weights, after first applying systematic offsets to values from Gray et al. (2003, 2006), in order to yield a homogenized data set. More details are discussed in Smith (2011), whose paper can also be resorted to for a discussion of possible time variability in the H and K emission, as well as references to a number of other smaller literature sources that were used. All of those stars with Ca II H and K indices can also be found in the TESS Input Catalog (Stassun et al. 2017).

An HR-diagram for the CATSUP stars for which Ca II H and K emission has been measured is shown in Fig. 5, where the datapoints have been coded on a continuous color-scale according to the value of the $\log R'_{HK}$ emission parameter. This figure illustrates the main-sequence nature of the majority of the CATSUP stars. There are some more-evolved stars that scatter by up to ~ 0.5 dex in $\log(L/L_{\odot})$ above the main sequence. Among solar-type dwarfs with $T_{\text{eff}} > 5400$ K these more-evolved stars tend to exhibit relatively low levels of Ca

II H and K emission $\log R'_{HK} < -4.8$. Relatively few dwarfs cooler than 5400 K in Fig. 5 are found to have such low levels of activity. Consequently, the values of $-4.8 < \log R'_{HK} < -4.5$ that do dominate among the more-evolved CATSUP stars in the solar-like temperature regime can be considered closer to the lower levels of activity encountered in the cooler CATSUP stars. Wright et al. (2004) found that many so-called “Maunder Minimum” stars of near-solar temperature but of notably lower activity levels than the average Sun, are in fact slightly evolved from the main sequence. The distribution of CATSUP stars with $\log R'_{HK} < -4.9$ seems consistent with the findings in Wright et al. (2004).

The distribution of chromospheric activity within the CATSUP sample is shown in Fig. 6. The pioneering work of Vaughan & Preston (1980) indicated a bimodal distribution among nearby dwarf stars, with high and low activity groups being separated by the so-called Vaughan-Preston gap. This gap can also be seen in samples discussed by Middelkoop (1982); Noyes et al. (1984); Soderblom (1985). A bimodality was evinced in the R_{HK} surveys of Henry et al. (1996) and Gray et al. (2006). The survey of southern hemisphere stars by Jenkins et al. (2008) found that the gap corresponded to a relatively low percentage of stars with activity levels of $\log R'_{HK} \sim -4.7$, while active and inactive stars had mean levels of -4.5 and -5.0 respectively. While a corresponding low-activity peak at $\log R'_{HK} \sim -4.9$ is seen for the CATSUP distribution in Fig. 6, a possible high activity peak near ~ -4.4 is quite muted. Within the CATSUP sample the Vaughan-Preston gap does seem to be relatively well populated, with a broad continuous distribution extending across the activity range from -4.8 to -4.3 .

Gray et al. (2006) found that the distribution of $\log R'_{HK}$ differs between stars of different metallicities, with a bimodality largely being confined to dwarfs with $[\text{M}/\text{H}] > -0.2$ dex. Within Fig. 6 we have similarly divided the CATSUP sample into metallicity groupings of $[\text{Fe}/\text{H}]$ less than or greater than -0.2 dex. The more metal-rich bin within CATSUP is not as strikingly bimodal as that shown in Fig. 5 of Gray et al. (2006), while the metal-poorer distribution in our Fig. 6 is similar to that found in their Fig. 5. Stars above the Vaughan-Preston gap are thus largely of metallicity similar to the Sun, while dwarfs with $[\text{Fe}/\text{H}] < -0.2$ dex constitute a significant component of the low-activity peak.

7. UV PHOTOMETRY WITH GALEX

An additional stellar activity measure critical to the understanding of exoplanets is the UV light from host stars. As the high energy UV photons alter the planets’ atmospheric evolution and photochemistry, interpretations of exoplanetary spectra are affected for both close-in giant planets and habitable zone earths (Miguel & Kaltenegger 2014; Rugheimer et al. 2015; Luger & Barnes 2015; Arney et al. 2016). We cross-correlated the CATSUP target catalog with the archived UV photometry of the GALEX space mission from the General Release¹¹ GR6/7. The GALEX satellite imaged roughly two-thirds of the sky from 2003 to

¹¹ The GALEX GR6/7 is available at <http://mastweb.stsci.edu/gcasjobs/>

2013 in two UV bands: the NUV (1750-2750 Å) and FUV (1350-1750 Å). The full description of the instrument and its mission is provided by Morrissey et al. (2005) and of the pipeline by Morrissey et al. (2007). The failure of the FUV detector in 2009 resulted in only NUV imaging for all observations after this date. We queried the GALEX archive for all stars in the catalog using a search radius of 30".

The NUV detector response becomes non-linear beyond 34 counts per second, which occurred for 102 (11%) of the CATSUP targets. In the case of non-linearity for these NUV measurements, we report the pipeline’s measured flux density as a lower limit, and Shkolnik (2013) was used as a reference for upper limits for bright targets in GALEX. In the FUV, the detector’s response becomes non-linear beyond 108 counts per second, but only affected a tiny fraction of the CATSUP stars. GALEX did not detect 309 (32%) of the stars in the FUV for which we report estimated upper limits. Flux densities, including their upper limits in the case of non-detection and lower-limits in the case of non-linear detector response are listed in Table 6. If a star’s NUV or FUV emission was detected by GALEX, but it was unable to be measured completely due to limited field of view, the data were deemed unreliable and excluded from the final catalog. There are 708 stars with UV measurements within CATSUP, where 676 of those stars can also be found in the TESS Input Catalog (Stassun et al. 2017).

In Fig. 7, we show a plot of the effective temperature (T_{eff}) with respect to the logged fluxes for both the FUV (blue) and NUV (red) with individual error bars. When T_{eff} is below 5500 K, the FUV scatters due to the interference with the star’s corona, namely that coronal interference is higher than the blackbody curve. Above $T_{\text{eff}} = 5500$ K, the FUV flux is dominated by the photosphere, which is temperature dependent. As the photosphere becomes a smaller fraction of the total FUV bandpass, the flux is increasingly from the chromosphere, the transition region, and the corona, which is dominated by stellar activity and not effective temperature. The NUV is only well detected when $T_{\text{eff}} < 5200$ K, hence the sharp cutoff for the red data points. This temperature cutoff also affects the number of data points in the $[F_{\text{FUV}}/F_{\text{NUV}}]_G$ relation, or the ratio of the flux densities in FUV and NUV band passes in GALEX, shown on the right in Fig. 7. The trend towards higher ratios with smaller effective temperature is due to the rapid reduction in NUV photons from the stellar photosphere. The large range in the UV ratio at a given temperature is due to variations in stellar activity. Per Fig. 7, we note that ~ 10 stars have $T_{\text{eff}} < 3900$ K, the typical cutoff between K and M dwarfs. We have confirmed that their effective temperatures are accurate, such that in nearly all cases, these stars were measured by multiple sources that gave similar temperatures. Since there are no obvious reasons for excluding these stars, we have opted to keep them within CATSUP.

Smith & Redenbaugh (2010) and Findeisen et al. (2011) showed the GALEX FUV magnitude of FGK dwarfs was sensitive to the level of stellar activity as judged from the strength of the Ca II H and K emission lines. The CATSUP stars also verify this result. Figure 8 presents a two-color B-V diagram for CAT-

SUP stars for which GALEX measurements of FUV magnitude have been made. It shows a hybrid color denoted FUV-V, which is obtained by combining the GALEX FUV magnitude and Johnson V magnitude (following the precepts of Findeisen et al. 2011), plotted against Johnson B-V color. To bring out the variation of FUV brightness with stellar activity, the data points have color-coded according to the categories defined by Henry et al. (1996), namely, $\log R'_{\text{HK}} \leq -5.1$ (very inactive), $-5.1 < \log R'_{\text{HK}} \leq -4.75$ (inactive), $-4.75 < \log R'_{\text{HK}} \leq -4.2$ (active), $\log R'_{\text{HK}} > -4.2$ (very active). Only a few CATSUP stars fall in the very inactive category, but the other three activity categories are well represented (Fig. 6). Specifically, of the CATSUP stars that had $\log R'_{\text{HK}}$ measurements, 3% are categorized as very active, 47% are active, 49% are inactive, and 1% are very inactive. These three categories occupy distinct regions of Fig. 8, and there are clear differences in the FUV-V color among them at a given B-V. As the degree of chromospheric activity increases, the values of the FUV-V color decreases due to increasing flux in the GALEX FUV band arising from stellar active regions. An interested reader is referred to the papers by Smith & Redenbaugh (2010) and Findeisen et al. (2011) for much more detail about this trend.

8. X-RAY DATA

X-ray fluxes, luminosities, and fractional luminosities were based on observations with the *Chandra*, *XMM*, and *ROSAT* missions. The derived X-ray fluxes were converted to a common energy band (*ROSAT*) to facilitate intercomparison of the various X-ray indices. Additionally, *ROSAT* was used as a baseline since much previous work explored rotation-activity relations and age dating using X-ray luminosities from that mission (Mamajek & Hillenbrand 2008; Wright et al. 2011).

8.1. *Chandra*

The *Chandra X-ray Observatory* provides X-ray imaging in peak energy range ~ 0.5 -7.0 keV, with sub-arcsecond point spread function, over a ~ 60 -250 arcmin² field of view (Weisskopf et al. 2000). We initially queried the CATSUP catalog (J2000 positions from SIMBAD) against the *Chandra* Source Catalog, Release 1.1 (Evans et al. 2010, 2014), which catalogued X-ray sources in imagery from the Advanced CCD Imaging Spectrometer (ACIS; Garmire et al. 2003). *Chandra* positions have astrometric accuracy better than $\sim 1''^{12}$, and broadband fluxes (“b”) in the 0.5-7.0 keV were recorded. Vetting of the *Chandra* X-ray counterparts against the optical astrometry yielded 11 reliable matches.

8.2. *XMM*

X-ray Multi-Mirror Mission (XMM-Newton) European Photon Imaging Camera (EPIC) (Strüder et al. 2001) has field of view 30' and covers the energy range 0.15-15 keV with moderate angular resolution ($\sim 6''$). A query of the CATSUP database (J2000 SIMBAD positions) with the 3XMM-DR5 catalog of serendipitously detected X-ray sources (Rosen et al. 2016) yielded 54 X-ray sources within 90". To ease comparison with the *ROSAT* X-ray

¹² <http://cxc.harvard.edu/cal/ASPECT/celmon/>

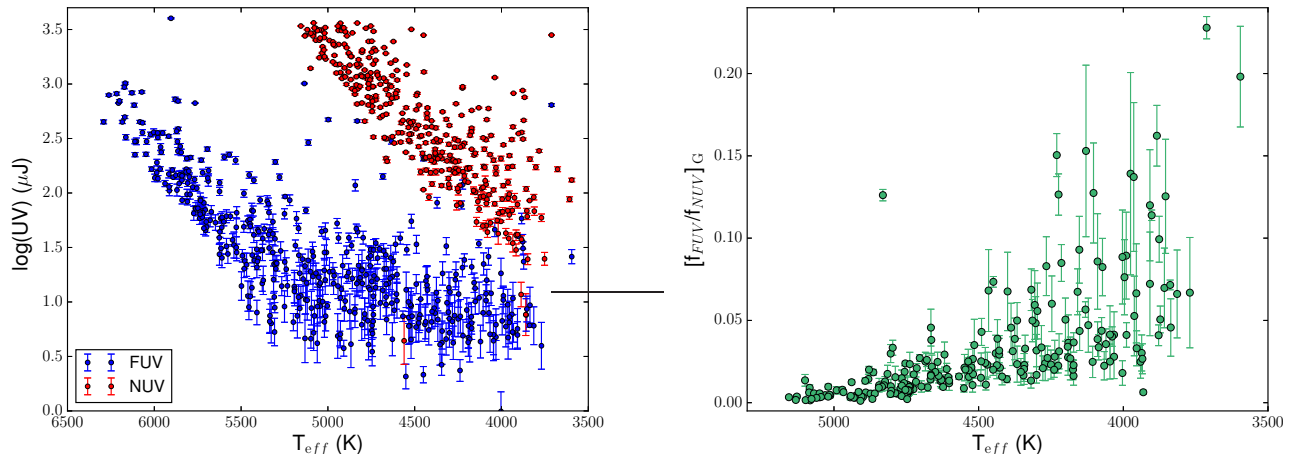


FIG. 7.— Left: The log of the FUV (blue) and NUV (red) GALEX fluxes with respect to effective temperature, T_{eff} . The NUV data are cut off at $T_{\text{eff}} < 5200$ K due to non-linearity in the detector for bright stars. Right: The ratio of the flux densities in the FUV and NUV GALEX band passes with respect to effective temperature, T_{eff} .

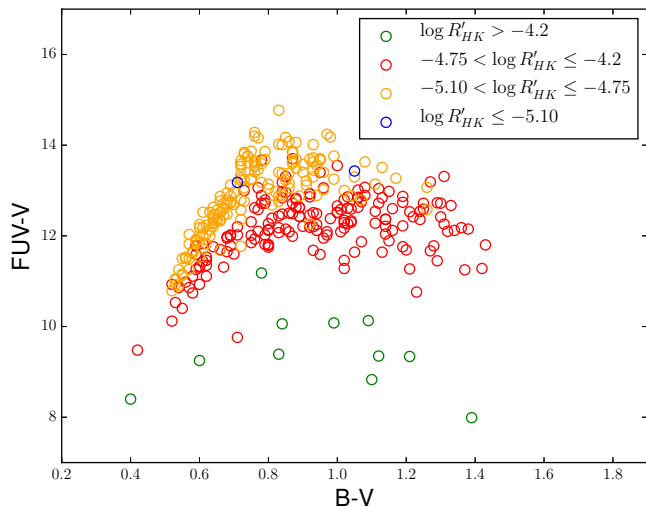


FIG. 8.— A two-color, B-V, diagram for CATSUP stars for which GALEX data are available. FUV-V is a hybrid color combining the GALEX FUV magnitude and Johnson V magnitude. Data points are color-coded according to the chromospheric activity categories defined by Henry et al. (1996). There are few stars in the very inactive category, but the other three activity categories are well represented and have clear differences in the FUV-V color at a given B-V.

fluxes, the XMM fluxes in bands 1, 2, and 3 were added, covering 0.2-2.0 keV.

8.3. ROSAT

ROSAT (ROentgen SATellite) conducted the *ROSAT All-Sky Survey* (RASS Voges et al. 1999, 2000) during a half-year period shortly after launch in 1990. The RASS mapped 99.7% of the sky with exposure times over 50 seconds in the 0.1-2.4 keV band with the Po-

sition Sensitive Proportional Counter (PSPC), and catalogued 18,811 sources down to an approximate limiting count-rate of 0.05 cts s^{-1} (Voges et al. 1999) in the Bright Source Catalog (RASS-BSC; 1RXS). The faint star extension of the RASS was published as the Faint Source Catalog (RASS-FSC) of 105,924 X-ray sources (Voges et al. 2000). A reanalysis of the RASS was recently completed by Boller et al. (2016), which resulted in a catalog of 135,000 X-ray sources in the 2nd *ROSAT* All-Sky Survey source catalogue (2RXS). Until the future eROSITA mission completes its survey, the 2RXS provides the astronomical community with the deepest all-sky X-ray survey. We adopted the count-rates and hardness ratio (HR1) from Boller et al. (2016) to calculate the energy conversion factor and resultant X-ray flux in the 0.1-2.4 keV band using the linear trend from Fleming et al. (1995):

$$ECF = (8.31 + 5.30 \text{ HR1}) \times 10^{-12} \text{ erg cm}^{-2} \text{ ct}^{-1} \quad (1)$$

Both the original RASS analyses and the revised RASS catalog produced by Boller et al. have similar positional uncertainties of typically $\sim 13''$ (Boller et al. 2016). Experience has shown that an optimal search radius for matching optical stars with their RASS X-ray counterparts is $40''$ (Neuhaeuser et al. 1995). A larger search radius of $90''$ was employed in a few cases to retrieve matches for some of the nearest stars which had large proper motions.

The Second *ROSAT* PSPC Catalog (Rosat 2000) of X-ray sources detected in *pointed* PSPC observations was also queried with both a $40''$ and $90''$ search radius around the positions of the CATSUP stars. A total of 109 stars had X-ray sources both in the *ROSAT* All-Sky Survey and the Second *ROSAT* PSPC Catalog. As the pointed observations in the latter catalog had longer exposure times than the All-Sky Survey, we adopted the PSPC count rates and hardness ratios HR1 from the latter, and calculated soft X-ray fluxes using

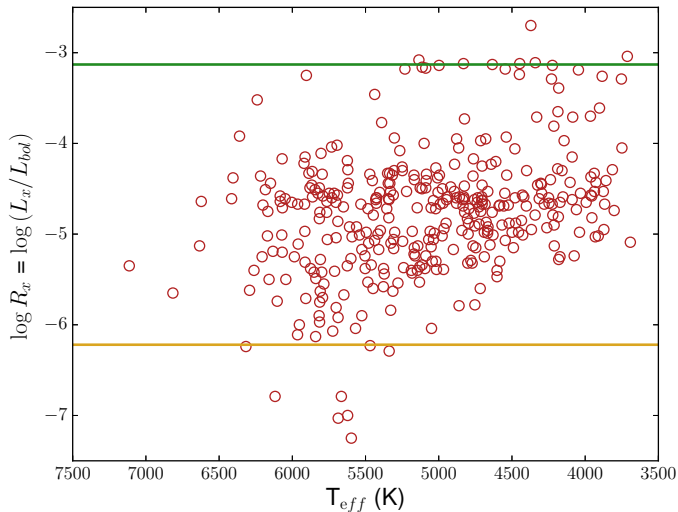


FIG. 9.— The fractional X-ray luminosity ($\log R_x$) with respect to effective temperature (T_{eff}) for stars within CATSUP. The yellow horizontal line is the solar coronal activity value and the green line is X-ray saturation per Wright et al. (2011).

the previously mentioned formula from (Fleming et al. 1995).

8.4. X-ray Flux Conversion

We would like the X-ray fluxes to be on a common system so that stellar activity levels can be usefully compared between stars. Comparison of the *XMM*, *Chandra*, and *ROSAT* fluxes amongst sources with detections in multiple surveys produced plots with large scatter (likely due to X-ray variability) and it was not clear that empirical flux conversions could be accurately estimated. We decided to use the WebPIMMS tool, or Portable, Interactive Multi-Mission Simulator¹³ (Mukai & Shiokawa 1993), to intercompare the X-ray fluxes between the observatories. For calculating X-ray flux conversions, we required an estimate of the H I column density. The median distance to the stars in the CATSUP catalog ($d < 30$ pc) is ~ 24 pc. Trends of hydrogen column density versus distance within the Local Bubble are consistent with neutral hydrogen densities of $n_H = 0.1 \text{ cm}^{-3}$ (Linsky et al. 2000). Hence for a mean distance of 24 pc for our sample stars, we adopt $\log N(\text{H I}) = 18.8$ as a representative hydrogen column density for the CATSUP sample for the webPIMMS tool.

The conversion between X-ray fluxes for one instrument and another depends on the temperature of the plasma, its chemical composition, and the intervening hydrogen column. Johnstone & Güdel (2015) demonstrated a strong correlation between coronal X-ray temperature and X-ray surface flux for main sequence stars with masses between ~ 0.2 and $\sim 1.1 M_{\odot}^N$: $\bar{T}_{\text{cor}} = 0.11 F_X^{0.26}$. The correlation spanned inactive stars such as the Sun at solar minimum ($T_X \simeq 1.0$ MK, $F_X \simeq 10^{3.65}$

$\text{ergs}^{-1} \text{cm}^{-2}$) to very active stars like 47 Cas B ($T_X \simeq 11$ MK, $F_X \simeq 10^{7.61} \text{ ergs}^{-1} \text{cm}^{-2}$). Indeed coronal temperatures scale much more closely with X-ray surface flux than with X-ray luminosity (L_X) or X-ray to bolometric luminosity ratio ($R_X = L_X/L_{\text{bol}}$). To produce self-consistent X-ray flux conversions between the *XMM*, *Chandra* and *ROSAT* data, we iteratively solve for a consistent combination of F_X and T_{cor} using the Johnstone & Güdel (2015) power law. An initial estimate of T_{cor} is adopted (1 MK), an initial conversion from *Chandra* or *XMM* X-ray flux to *ROSAT* flux is calculated using PIMMS at this temperature (adopting $\log N(\text{H I}) = 18.8$ and solar composition). Then, an initial X-ray surface flux (F_X) is calculated, and a revised coronal temperature T_{cor} is recalculated. This cycle is iterated until T_{cor} changes by less than 0.01 dex between iterations. The iterative method encountered a few troublesome cases for low T_{cor} that would not converge, all with $T_{\text{cor}} < 1$ MK. Based on the observed X-ray fluxes at solar minimum and that observed for coronal holes, we simply adopted $T_{\text{cor}} = 1$ MK for these cases.

The final converted fluxes, flux errors, luminosity, and activity from the *XMM*, *Chandra*, and *ROSAT* X-ray missions can be found in Table 6. A total of 364 stars have X-ray measurements within CATSUP, where 363 of those stars can also be found in the TESS Input Catalog (Stassun et al. 2017). A plot of the fractional X-ray luminosity $\log R_x = \log(L_x/L_{\text{bol}})$, using the median value of $\log R_x$ from the three missions, with respect to T_{eff} is show in Fig. 9. The yellow line is the coronal activity value of the Sun while the green line is the empirical X-ray saturation limit (Wright et al. 2011). The two lines show that the majority of the CATSUP stars (with X-ray measurements) fall within these two values and that the upper envelope is relatively constant across spectral types, which implies saturation. We also see that the cooler, lower mass stars are more active. The spread in the $\log R_x$ values is likely the result of different rotation rates, since it is expected that equal mass stars would have approximately the same bolometric luminosity.

As a consistency check, we searched Table 6 for stars with X-ray measurements from two different instruments, in order to compare their normalized fluxes. Among our sample, we find 22 stars with both *ROSAT* and *XMM* data, and three stars with both *ROSAT* and *Chandra* measurements. The derived flux values are plotted relative to one another in Fig. 10. For all points, the abscissa is the normalized flux from *ROSAT*, and the ordinate can be either flux from *XMM* (filled green) or *Chandra* (empty blue). The flux values generally show good agreement for the X-ray-brighter stars, suggesting that our normalization process is reliable when the fluxes are well measured. At the dimmer end, some stars deviate from the one-to-one line, a likely consequence of poorer counting statistics in the shallower *ROSAT* survey. However intrinsic fluctuations in the X-ray brightness, for example due to solar-type cycles, could also contribute.

9. APPLICATION

The CATSUP dataset combines a variety of properties for stars within 30 pc, such that individual stars as well as the solar neighborhood can be better characterized. To take advantage of the assorted available prop-

¹³ heasarc.gsfc.nasa.gov/cgi-bin/Tools/w3pimms/w3pimms.pl

TABLE 1
A SUMMARY OF THE VELOCITY COMPONENTS OF CATSUP STARS WITH DIFFERENT ACTIVITY LEVELS

	Very Active $x > -4.2$	Active $-4.75 < x \leq -4.2$	Inactive $-5.1 < x \leq -4.75$	Very Inactive $x \leq -5.1$
mean U	-12.40	-10.83	-13.69	1.96
std U	22.02	29.22	42.16	41.19
mean V	-22.81	-16.42	-28.81	-74.96
std V	17.25	18.91	29.99	48.14
mean W	-13.86	-8.76	-7.04	3.00
std W	13.85	13.86	23.64	13.45

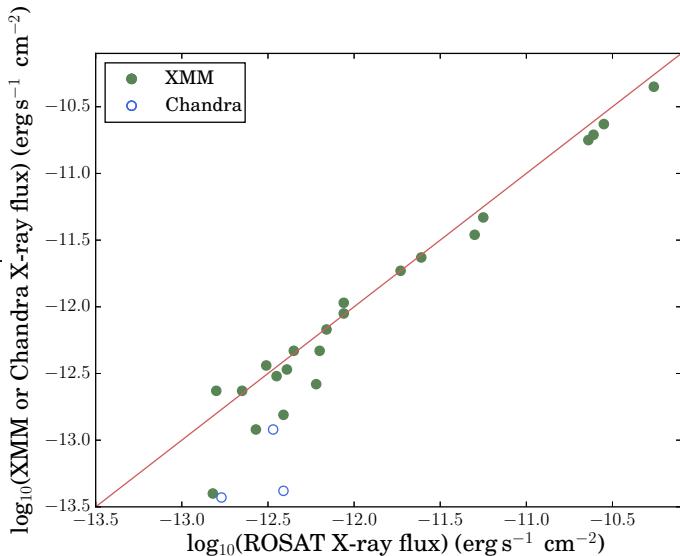


FIG. 10.— The X-ray flux from ROSAT (on the x-axis) with respect to X-ray flux measurements in the same star from XMM (green, closed circle) or Chandra (blue, open circle). A one-to-one line is overlaid in red.

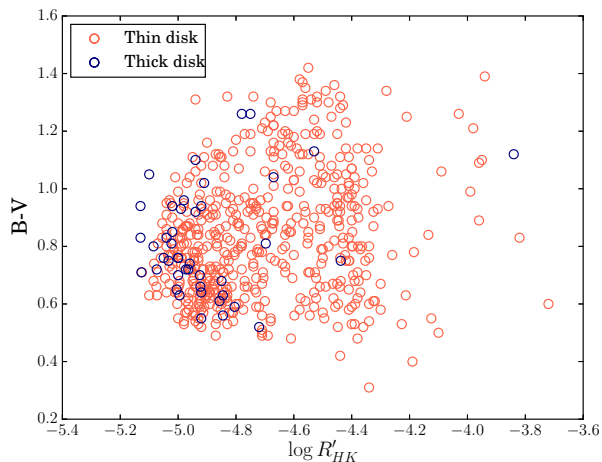


FIG. 11.— The Ca II H and K index, $\log R'_{HK}$, with respect to B-V color.

erties, we have plotted the Ca II H and K emission index $\log R'_{HK}$ with respect to both B-V color in Fig. 11. We have color-coded the stars to show the likely disk component of origin, where orange is thin disk and blue is thick disk, based on their kinematics per (Bensby et al. 2003; Hinkel et al. 2014). The thick disk stars are mainly concentrated around $\log R'_{HK}$ of $\sim -5.0 \pm 0.2$. In other words, they have emission indices comparable to the Sun – they are mostly very low activity. Along these lines, we considered whether the height above/below the Galactic plane (Z) and [Fe/H] correlate with a stellar activity index (that is sensitive to age). We did not see any trends with respect to $\log R'_{HK}$ vs. |Z|, or with respect to a multitude of abundances within both thin- and thick-disk stars, see Fig. 12. The conclusion that we can draw is that CATSUP stars encompass the full range of Z-height values in both the thin and thick disk subsets regardless of their level of Ca II H and K stellar activity indices (at least for $\log R'_{HK} < -4.8$ or so).

The thick disk stars typically have $\log R'_{HK} < -4.8$, and so fall in the low-activity grouping below the Vaughan-Preston gap (Vaughan & Preston 1980) in plots of Ca II H and K activity versus B-V. As such the thick disk stars populate the peak at $\log R'_{HK} \sim -4.9$ in Fig. 6. If the thick disk stars are removed from the histogram in Fig. 6, the resulting distribution for thin disk stars still shows a pronounced local maximum near -4.9 . Thus a high incidence of inactive stars is a property of the thin disk as well as the thick disk.

Looking at the two populations of stars in Fig. 11, there are 536 stars from the thin disk while 43 are from the thick disk ($\sim 8\%$). To better understand these two stellar populations, we utilize a two-sample Kolmogorov-Smirnov (KS) test which analyzes whether the two samples are drawn from the same distribution. If the p-value is below a certain significance level, typically 0.05, then the null hypothesis (that the two samples are from the same distribution) is rejected. Note, the p-value is not the probability of the null hypothesis being true or false. In other words, a p-value > 0.05 does not mean that the two samples are similar, it merely states that there was no evidence to show that the two samples were significantly different. This point is subtle and often misinterpreted within the literature. A two-sample KS test of the $\log R'_{HK}$ values for thin- and thick-disk stars yields a p-value = 2.02×10^{-7} – meaning that the two samples are statistically different.

We see in Fig. 11 that thick-disk stars have predominantly low values of $\log R'_{HK}$, typically $\log R'_{HK} < -4.8$. For all stars with $\log R'_{HK} < -4.8$, there are 233 stars from the thin disk and 35 from the thick disk ($\sim 15\%$).

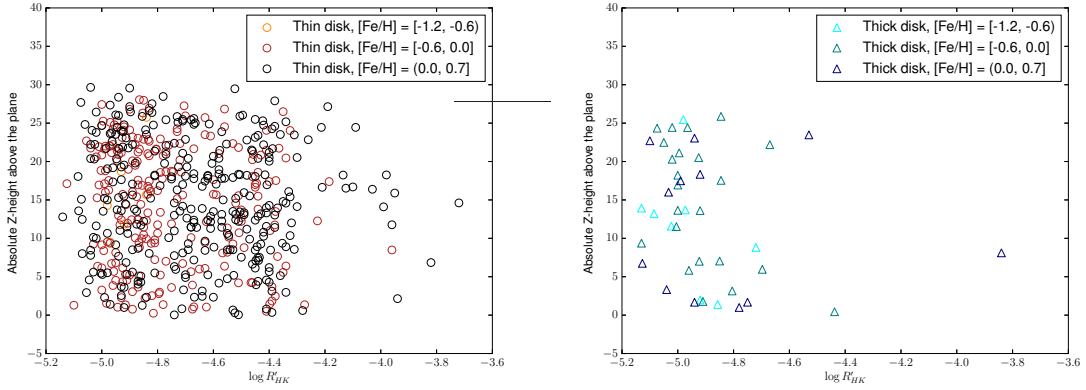


FIG. 12.— Stellar activity with respect to the absolute Z-height above the plane for $[\text{Fe}/\text{H}]$, where stars in the thin disk are shown on the left while stars in the thick disk are on the right.

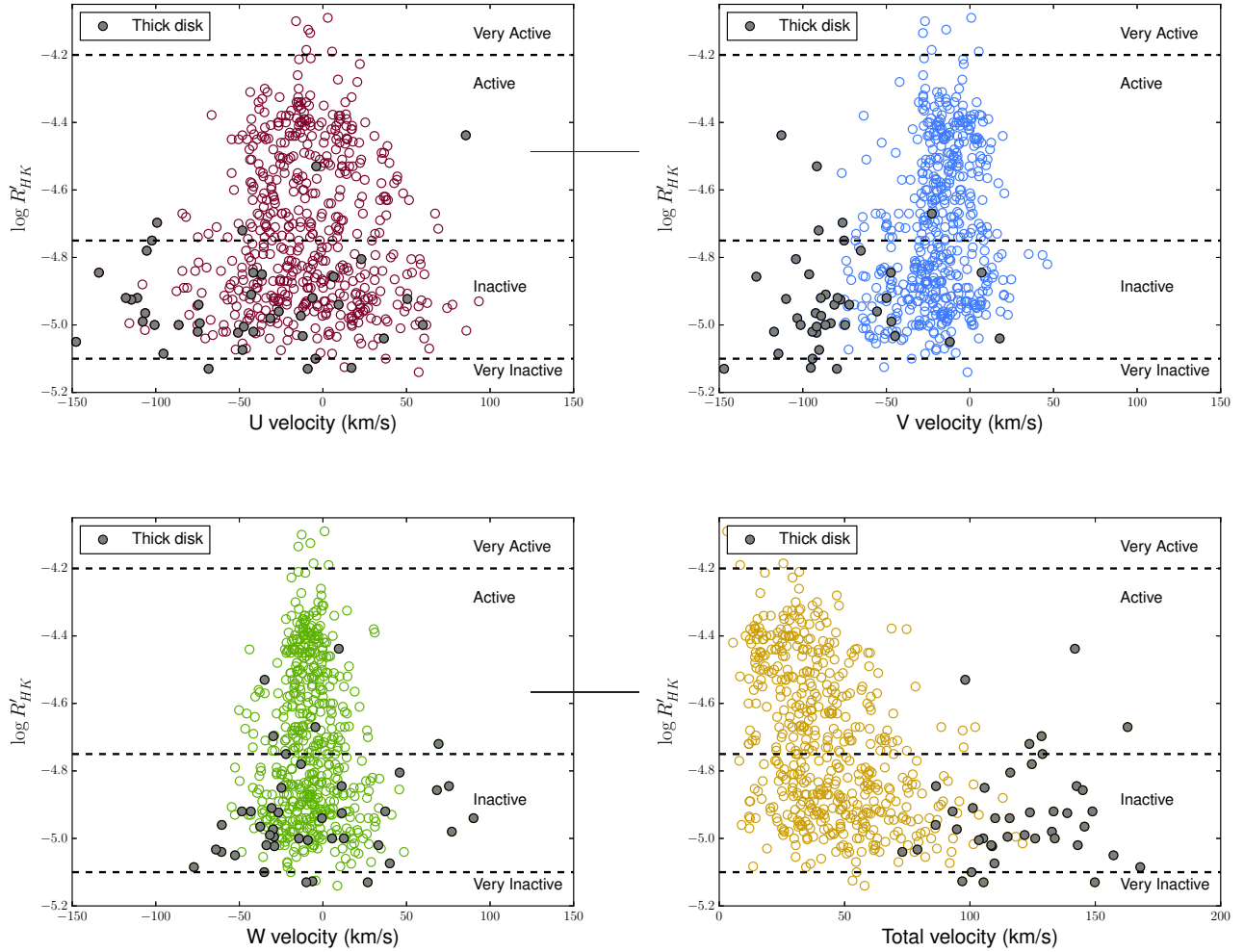


FIG. 13.— The chromospheric activity indicator $\log R'_{HK}$, based on the Ca II H and K emission lines, is plotted versus the U, V, and W velocity components of space motion as well as the total space velocity for stars in the CATSUP sample. Thick disk stars are depicted with filled symbols, thin disk stars with open circles. The four stellar activity groupings defined by Henry et al. (1996) are indicated by the horizontal dashed lines and labelled accordingly.

Doing a two-sample KS test on the $\log R'_{\text{HK}}$ values for thin- and thick-disk stars where $\log R'_{\text{HK}} < -4.8$ gives $p = 0.006$. Finally, we did a two-sample KS test for the $\log R'_{\text{HK}}$ values for those stars in the thick disk and with $\log R'_{\text{HK}} < -4.8$ (total 35 stars) with respect to the entire sample of thin-disk stars (total 536 stars) – the p-value is 2.82×10^{-11} .

Vaughan & Preston (1980) searched for kinematic differences among some 185 dwarfs with different levels of Ca II H and K activity. They found that for dwarfs of a given spectral type, groupings according to strong H and K emission (high activity) have smaller dispersions in the component of space motion perpendicular to the Galactic plane. Thus the chromospherically younger stars in their sample have different mean space motions than chromospherically older stars. Soderblom (1990) extended this work with a larger sample of chromospherically active solar-like, K, and M dwarfs, finding them to have kinematics consistent with a young population of age around 0.5-2 Gyr. The age dependence of space motion provides a tool for studying the dynamical evolution of the Galactic disk (e.g. Wielen 1974). As such any correlations between stellar kinematics and stellar activity are worth searching for among the CATSUP stars. Jenkins et al. (2011) have published a very thorough study of the correlations for solar-type dwarfs and subgiants, highlighting the utility of this approach.

The distributions of the (U,V,W) components of space motion of the CATSUP stars are shown in Fig. 13, with some summary characteristics being listed in Table 1. In the table the CATSUP stars have been divided into the four stellar activity groupings defined by Henry et al. (1996), as also adopted in Section 7, and for each grouping the mean value of each velocity component is listed along with the standard deviation. We leave the “very inactive” stars out of the discussion because of their small number within the CATSUP sample. In terms of the W component of velocity perpendicular to the Galactic plane, the velocity dispersion among the inactive stars is notably greater than among the active and very-active dwarfs. This is also the case for the standard deviations in the U and V components of motion. Thus overall the inactive stars evince a greater dispersion in all three velocity components than the active stars. This trend is partly but not entirely driven by the thick disk dwarfs within CATSUP. Inspection of Fig. 13 shows that these trends exist even within the thin disk population alone. The upper panels of Fig. 13 illustrate the offsets in mean U and V velocity between the thick and thin disk stars. Thus the CATSUP sample verifies and extends the early results of Vaughan & Preston (1980), and is consistent with the findings of Soderblom (1990) and Jenkins et al. (2011, see their Fig. 16 to which our Fig. 13 is analogous).

Ultimately, it seems that the thick-disk stars have predominantly low activity, and higher velocity dispersions on average toward or away-from the Galactic plane. The CATSUP set of thick-disk stars has a distinctly different distribution of chromospheric activity than the CATSUP thin-disk stars. We note as a caveat, however, that the number of thick disk stars in our sample is roughly an order of magnitude smaller than the thin-disk stars.

10. SUMMARY

We have assembled a dataset of stellar properties for 951 FGK-type stars within 30 pc of the Sun. Beginning with the Gaia TGAS subset of astrometric data, we have combined information regarding multiplicity within stellar systems (ExoCat), stellar abundance measurements (Hypatia), standardized spectral types, Ca II H and K stellar activity indices, NUV and FUV photometry from GALEX, and X-ray fluxes and luminosities from ROSAT, XMM, and Chandra. The aim of this project was to collate a wide variety of data for nearby stars such that they could be more easily characterized. The information available in CATSUP can be utilized for the direct sample or act as a proxy for similar stars, in order to better understand the overall trends within solar neighborhood stars as well as stars that host exoplanets. CATSUP was compiled in anticipation of upcoming exoplanet surveys such as TESS, CHEOPS, and WFIRST.

While we included data currently available within the literature, we also presented new stellar information. We explored the GALEX UV data and found that the FUV and NUV flux correlated strongly with effective temperature as the photospheres of hotter stars have bluer peaks in their Planck functions. At temperatures below 5500 K, the data show a much large range at a given T_{eff} due to higher contributions to the FUV emission from the more variable stellar corona and high chromosphere compared with hotter stars (see Fig. 7, left). At higher temperatures, the FUV flux is more linear with T_{eff} since it is dominated by the temperature dependent stellar photosphere. In general, the NUV data show a large range at a given effective temperature. When combined into a flux density ratio in the FUV and NUV band passes per Fig. 7 (right) the influence of the stellar corona/transition region/chromosphere over the photosphere at low temperatures is again present. Additionally, we analyzed how $\log R'_{\text{HK}}$ activity effected stellar spectral energy distributions, such that more active stars had bluer FUV-V colors.

X-ray data from multiple missions were combined per a new methodology that allowed all available X-ray information to be utilized for stellar characterization. The X-ray data were investigated with respect to effective temperature in Fig. 9. The majority of the stars were found to fall between the solar coronal activity and the X-ray saturation limit, where the latter was exemplified by a relatively constant $\log R_x$ across spectral types. Overall, the smaller, cool stars were found to have the highest fractional X-ray luminosity or coronal activity indicator. We compared the coronal activity ($\log R_x$) and chromospheric activity ($\log R'_{\text{HK}}$) in the same manner as Mamajek & Hillenbrand (2008), see Fig. 14. We found a similar correlation with respect to a linear trend, where the overlaid line is defined as $y = 0.28687x - 3.1668$, and range in data.

Finally, we examined the correlation between stars in the CATSUP sample that are likely to have originated from the thick disk (see Section 4) and the Ca II H and K index $\log R'_{\text{HK}}$. We found that the thick-disk stars had a chromospheric activity that was preferentially $\log R'_{\text{HK}} < -4.8$ in Fig 11. Compared with the thin-disk stars, these kinematic stellar sub-groups within CATSUP were statistically different per a two-sample KS test. When analyzing $\log R'_{\text{HK}}$ with respect to UVW galactic velocity, the lower activity stars had greater dispersion in the

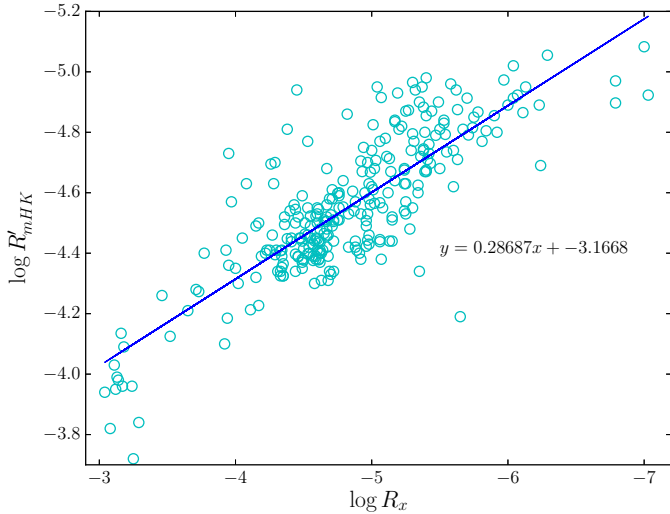


FIG. 14.— The Ca II H and K indices with respect to the fractional X-ray luminosity, where $\log R_x = \log(L_x/L_{bol})$. A linear regression line is overlaid in blue, with the equation given. The scatter is usual for a sample of stars such as CATSUP.

three individual galactic velocity components, a trend which is not wholly attributable to the presence of thick-disk stars.

While there are a number of additional trends to be found between the 951 CATSUP stars, we leave this task to future papers either by the ASU NExSS team or other

colleagues. The properties within CATSUP were strategically combined in order to maximize characterization of nearby main-sequence stars. It is our goal that by knowing more about stars from both a physical and chemical perspective, we will enable a greater understanding of the solar neighborhood. Additionally, we hope that CATSUP will help inform either target selection or follow-up observations for the TESS, CHEOPS, and WFIRST missions.

ACKNOWLEDGEMENTS

The results reported herein benefited from collaborations and/or information exchange within NASA's Nexus for Exoplanet System Science (NExSS) research coordination network sponsored by NASA's Science Mission Directorate. NRH would like to thank CHW3 and Tatertot, who goes well with CATSUP. NRH and GES acknowledge the support of the Vanderbilt Office of the Provost through the Vanderbilt Initiative in Data-intensive Astrophysics (VIDA) fellowship. EO and ES appreciate support from NASA/Habitable Worlds grant NNX16AB62G. GHS wishes to acknowledge the support of NSF Award 1517791. Part of this research was carried out at the Jet Propulsion Laboratory, California Institute of Technology, under a contract with NASA. This document does not contain any export controlled technical data (URS268608). Finally, this research has made use of the VizieR catalogue access tool, CDS, Strasbourg, France as well as Filtergraph (for the HR diagram), an online data visualization tool developed at Vanderbilt University through the Vanderbilt Initiative in Data-intensive Astrophysics (VIDA).

REFERENCES

- Adibekyan, V., Delgado-Mena, E., Figueira, P., et al. 2016, *A&A*, 592, A87
- Anders, E., & Grevesse, N. 1989, *Geochimica et Cosmochimica Acta*, 53, 197
- Anderson, E., & Francis, C. 2012, *Astronomy Letters*, 38, 331
- Arenou, F., Luri, X., Babusiaux, C., et al. 2017, *A&A*, 599, A50
- Arney, G., Domagal-Goldman, S. D., Meadows, V. S., et al. 2016, *Astrobiology*, 16, 873
- Asplund, M., Grevesse, N., Sauval, A. J., & Scott, P. 2009, *ARA&A*, 47, 481
- Astraatmadja, T. L., & Bailer-Jones, C. A. L. 2016, *ApJ*, 833, 119
- Batalha, N. M., Rowe, J. F., Bryson, S. T., et al. 2013, *ApJS*, 204, 24
- Battistini, C., & Bensby, T. 2016, *A&A*, 586, A49
- Baumann, P., Ramírez, I., Meléndez, J., Asplund, M., & Lind, K. 2010, *A&A*, 519, A87
- Bensby, T., Feltzing, S., & Lundström, I. 2003, *A&A*, 410, 527
- Blanco-Cuaresma, S., Soubiran, C., Heiter, U., & Jofré, P. 2014, *A&A*, 569, A111
- Boller, T., Freyberg, M. J., Trümper, J., et al. 2016, *A&A*, 588, A103
- Brewer, J. M., Fischer, D. A., Valenti, J. A., & Piskunov, N. 2016, *ApJS*, 225, 32
- Burger, D., Stassun, K. G., Pepper, J., et al. 2013, *Astronomy and Computing*, 2, 40
- Chen, Y. Q., Nissen, P. E., Benoni, T., & Zhao, G. 2001, *A&A*, 371, 943
- da Silva, R., Milone, A. d. C., & Rocha-Pinto, H. J. 2015, *A&A*, 580, A24
- Delgado Mena, E., Israelian, G., González Hernández, J. I., et al. 2014, *A&A*, 562, A92
- Delgado Mena, E., Bertrán de Lis, S., Adibekyan, V. Z., et al. 2015, *A&A*, 576, A69
- Dressing, C. D., & Charbonneau, D. 2013, *ApJ*, 767, 95
- Evans, I. N., Primi, F. A., Glotfelty, K. J., et al. 2010, *ApJS*, 189, 37
- Evans, I. N., Primi, F. A., Glotfelty, C. S., et al. 2014, *VizieR Online Data Catalog*, 9045
- Fabrizius, C., Høg, E., Makarov, V. V., et al. 2002, *A&A*, 384, 180
- Findeisen, K., Hillenbrand, L., & Soderblom, D. 2011, *AJ*, 142, 23
- Fleming, T. A., Molendi, S., Maccacaro, T., & Wolter, A. 1995, *ApJS*, 99, 701
- Gaia Collaboration, Brown, A. G. A., Vallenari, A., et al. 2016, *A&A*, 595, A2
- Garmire, G. P., Bautz, M. W., Ford, P. G., Nousek, J. A., & Ricker, Jr., G. R. 2003, in *Proc. SPIE*, Vol. 4851, X-Ray and Gamma-Ray Telescopes and Instruments for Astronomy., ed. J. E. Truemper & H. D. Tananbaum, 28–44
- Ghezzi, L., Cunha, K., Smith, V. V., & de la Reza, R. 2010, *The Astrophysical Journal*, 724, 154
- Gomes da Silva, J., Santos, N. C., Boisse, I., Dumusque, X., & Lovis, C. 2014, *A&A*, 566, A66
- Gonzalez, G. 2014, *Monthly Notices of the Royal Astronomical Society*, 441, 1201
- . 2015, *Monthly Notices of the Royal Astronomical Society*, 446, 1020
- Gonzalez, G., Carlson, M. K., & Tobin, R. W. 2010, *Monthly Notices of the Royal Astronomical Society*, 403, 1368
- Gonzalez, G., Carlson, M. K., & Tobin, R. W. 2010, *MNRAS*, 407, 314
- Gonzalez, G., Laws, C., Tyagi, S., & Reddy, B. E. 2001, *AJ*, 121, 432
- Gray, D. F. 1997, *Nature*, 385, 795
- Gray, R. O., Corbally, C. J., Garrison, R. F., et al. 2006, *AJ*, 132, 161
- Gray, R. O., Corbally, C. J., Garrison, R. F., McFadden, M. T., & Robinson, P. E. 2003, *AJ*, 126, 2048
- Gustafsson, B., Bell, R. A., Eriksson, K., & Nordlund, A. 1975, *A&A*, 42, 407

- Hartmann, L., Soderblom, D. R., Noyes, R. W., Burnham, N., & Vaughan, A. H. 1984, *ApJ*, 276, 254
- Henry, T. J., Soderblom, D. R., Donahue, R. A., & Baliunas, S. L. 1996, *AJ*, 111, doi:10.1086/117796
- Henry, T. J., Walkowicz, L. M., Barto, T. C., & Golimowski, D. A. 2002, *AJ*, 123, 2002
- Hinkel, N. R., Timmes, F. X., Young, P. A., Pagano, M. D., & Turnbull, M. C. 2014, *AJ*, 148, 54
- Hinkel, N. R., Young, P. A., Pagano, M. D., et al. 2016, *ApJS*, 226, 4
- Houk, N., & Cowley, A. P. 1975, University of Michigan Catalogue of two-dimensional spectral types for the HD stars. Volume I. Declinations -90 to -53 (Dept. of Astronomy, University of Michigan)
- Israelian, G., Santos, N. C., Mayor, M., & Rebolo, R. 2004, *Astronomy and Astrophysics*, 414, 601
- Israelian, G., Mena, E. D., Santos, N. C., et al. 2009, *Nature*, 462, 189
- Jenkins, J. S., Jones, H. R. A., Pavlenko, Y., et al. 2008, *A&A*, 485, 571
- Jenkins, J. S., Jones, H. R. A., Tinney, C. G., et al. 2006, *MNRAS*, 372, 163
- Jenkins, J. S., Murgas, F., Rojo, P., et al. 2011, *A&A*, 531, A8
- Johnson, M. C., Endl, M., Cochran, W. D., et al. 2016, *ApJ*, 821, 74
- Johnstone, C. P., & Güdel, M. 2015, *A&A*, 578, A129
- Keenan, P. C., & McNeil, R. C. 1989, *ApJS*, 71, 245
- Kurucz, R. L. 1993, *SYNTHES* spectrum synthesis programs and line data (Cambridge, MA: Smithsonian Astrophysical Observatory, —c1993)
- Lambert, D. L., Heath, J. E., & Edvardsson, B. 1991, *MNRAS*, 253, 610
- Lambert, D. L., & Reddy, B. E. 2004, *Monthly Notices of the Royal Astronomical Society*, 349, 757
- Linsky, J. L., Redfield, S., Wood, B. E., & Piskunov, N. 2000, *ApJ*, 528, 756
- Liu, Y. J., Tan, K. F., Wang, L., et al. 2014, *The Astrophysical Journal*, 785, 94
- Lodders, K., Plame, H., & Gail, H.-P. 2009, *Abundances of the Elements in the Solar System*, Vol. 4B (Berlin, Heidelberg, New York: Springer-Verlag), 44
- López-Valdivia, R., Bertone, E., & Chávez, M. 2017, *Monthly Notices of the Royal Astronomical Society*, stx249
- Luck, R. E. 2015, *The Astronomical Journal*, 150, 88
- 2017, *The Astronomical Journal*, 153, 21
- Luck, R. E., & Heiter, U. 2006, *AJ*, 131, 3069
- 2007, *AJ*, 133, 2464
- Luger, R., & Barnes, R. 2015, *Astrobiology*, 15, 119
- Mahdi, D., Soubiran, C., Blanco-Cuaresma, S., & Chemin, L. 2016, *A&A*, 587, A131
- Maldonado, J., Eiroa, C., Villaver, E., Montesinos, B., & Mora, A. 2015, *Astronomy & Astrophysics*, 579, A20
- Maldonado, J., & Villaver, E. 2016, *A&A*, 588, A98
- Mallik, S. V., Parthasarathy, M., & Pati, A. K. 2003, *Astronomy and Astrophysics*, 409, 251
- Mamajek, E. E., & Hillenbrand, L. A. 2008, *ApJ*, 687, 1264
- Mason, B. D., Wycoff, G. L., Hartkopf, W. I., Douglass, G. G., & Worley, C. E. 2001, *AJ*, 122, 3466
- Mayor, M., Marmier, M., Lovis, C., et al. 2011, *ArXiv e-prints*, arXiv:1109.2497
- Mennesson, B., Gaudi, S., Seager, S., et al. 2016, in *Space Telescopes and Instrumentation 2016: Optical, Infrared, and Millimeter Wave*, ed. H. A. MacEwen, G. G. Fazio, M. Lystrup, N. Batalha, N. Siegler, & E. C. Tong (SPIE)
- Middelkoop, F. 1982, *A&A*, 107, 31
- Miguel, Y., & Kaltenegger, L. 2014, *ApJ*, 780, 166, 13 pp
- Mishenina, T., Kovtyukh, V., Soubiran, C., & Adibekyan, V. Z. 2016, *MNRAS*, 462, 1563
- Mishenina, T. V., Soubiran, C., Kovtyukh, V. V., Katsova, M. M., & Livshits, M. A. 2012, *A&A*, 547, A106
- Morrissey, P., Schiminovich, D., Barlow, T. A., et al. 2005, *ApJL*, 619, L7
- Morrissey, P., Conrow, T., Barlow, T. A., et al. 2007, *ApJS*, 173, 682
- Mukai, K., & Shiokawa, K. 1993, *ApJ*, 418, 863
- Neuhäuser, R., Sterzik, M. F., Schmitt, J. H. M. M., Wichmann, R., & Krautter, J. 1995, *A&A*, 297, 391
- Nissen, P. E. 2013, *Astronomy & Astrophysics*, 552, A73
- Nissen, P. E. 2016, *A&A*, 593, A65
- Notsu, Y., Honda, S., Maehara, H., et al. 2017, *PASJ*, 69, 12
- Noyes, R. W., Hartmann, L. W., Baliunas, S. L., Duncan, D. K., & Vaughan, A. H. 1984, *ApJ*, 279, 763
- Ochsenbein, F., Bauer, P., & Marcout, J. 2000, *A&AS*, 143, 23
- Pagano, M., Young, P. A., & Challa, P. 2017, *ApJ*, in review
- Pecaut, M. J., & Mamajek, E. E. 2016, *MNRAS*, 461, 794
- Prša, A., Harmanec, P., Torres, G., et al. 2016, *AJ*, 152, 41
- Ramírez, I., Allende Prieto, C., & Lambert, D. L. 2013, *ApJ*, 764, 78
- Ramírez, I., Fish, J. R., Lambert, D. L., & Prieto, C. A. 2012, *The Astrophysical Journal*, 756, 46
- Reddy, B., Tomkin, J., Lambert, D., & Prieto, C. A. 2003, *MNRAS*, 340, 304
- Reetz, J. K. 1991, PhD thesis, Ludwig-Maximilians-Universität München
- Reis, W., Corradi, W., de Avillez, M. A., & Santos, F. P. 2011, *ApJ*, 734, 8
- Rosat, C. 2000, *VizieR Online Data Catalog*, 9030
- Rosen, S. R., Webb, N. A., Watson, M. G., et al. 2016, *A&A*, 590, A1
- Rugheimer, S., Kaltenegger, L., Segura, A., Linsky, J., & Mohanty, S. 2015, *ApJ*, 809, 57
- Seager, S., Turnbull, M., Sparks, W., et al. 2015, in *Techniques and Instrumentation for Detection of Exoplanets VII*, ed. S. Shaklan (SPIE)
- Shkolnik, E. L. 2013, *ApJ*, 766, 9
- Showman, A. P., & Malhotra, R. 1999, *Science*, 296, 77
- Smith, G. 2011, *The Observatory*, 131, 1
- Smith, G. H., & Redenbaugh, A. K. 2010, *PASP*, 122, 1303
- Snedden, C. A. 1973, PhD thesis, The University of Texas - Austin
- Soderblom, D. R. 1985, *AJ*, 90, 2103
- 1990, *AJ*, 100, 204
- Soderblom, D. R., Duncan, D. K., & Johnson, D. R. H. 1991, *ApJ*, 375, 722
- Soubiran, C., Le Campion, J.-F., Brouillet, N., & Chemin, L. 2016, *A&A*, 591, A118
- Spergel, D., Gehrels, N., Breckinridge, J., et al. 2013, *ArXiv e-prints*, arXiv:1305.5422
- Spergel, D., Gehrels, N., Baltay, C., et al. 2015, *ArXiv e-prints*, arXiv:1503.03757
- Stassun, K. G., Oelkers, R. J., Pepper, J., et al. 2017, *ArXiv e-prints*, arXiv:1706.00495
- Strüder, L., Briel, U., Dennerl, K., et al. 2001, *A&A*, 365, L18
- Suárez-Andrés, L., Israelian, G., González Hernández, J. I., et al. 2016, *A&A*, 591, A69
- Takeda, Y., Honda, S., Kawanomoto, S., Ando, H., & Sakurai, T. 2010, *Astronomy and Astrophysics*, 515, A93
- Takeda, Y., & Kawanomoto, S. 2005, *PASJ*, 57, 45
- Takeda, Y., Taguchi, H., Yoshioka, K., et al. 2007, *PASJ*, 59, 1127
- Taylor, M. B. 2005, in *Astronomical Society of the Pacific Conference Series*, Vol. 347, *Astronomical Data Analysis Software and Systems XIV*, ed. P. Shopbell, M. Britton, & R. Ebert, 29
- Trevisan, M., & Barbuy, B. 2014, *Astronomy & Astrophysics*, 570, A22
- Trevisan, M., Barbuy, B., Eriksson, K., et al. 2011, *A&A*, 535, 42
- Tucci Maia, M., Ramírez, I., Meléndez, J., et al. 2016, *A&A*, 590, A32
- Turnbull, M. C. 2015, *ArXiv e-prints*, arXiv:1510.01731
- Unterborn, C. T., Dismukes, E. E., & Panero, W. R. 2016, *ApJ*, 819, 32
- Valenti, J. A., & Fischer, D. A. 2005, *ApJS*, 159, 141
- Vaughan, A. H., & Preston, G. W. 1980, *PASP*, 92, 385
- Voges, W., Aschenbach, B., Boller, T., et al. 1999, *A&A*, 349, 389
- 2000, *IAU Circ.*, 7432
- Vogt, S. S., Burt, J., Meschiari, S., et al. 2015, *ApJ*, 814, 12
- Wanke, H. 1981, *Philosophical Transactions of the Royal Society of London Series A*, 303, 287
- Weisskopf, M. C., Tananbaum, H. D., Van Speybroeck, L. P., & O'Dell, S. L. 2000, in *Proc. SPIE*, Vol. 4012, *X-Ray Optics, Instruments, and Missions III*, ed. J. E. Truemper & B. Aschenbach, 2–16
- Wielen, R. 1974, *Highlights of Astronomy*, 3, 395
- Wilson, O. C. 1978, *ApJ*, 226, 379

- Wright, J. T., Marcy, G. W., Butler, R. P., & Vogt, S. S. 2004, ApJS, 152, 261
- Wright, N. J., Drake, J. J., Mamajek, E. E., & Henry, G. W. 2011, ApJ, 743, 48
- Yan, H. L., Shi, J. R., Nissen, P. E., & Zhao, G. 2016, Astronomy & Astrophysics, 585, A102
- Ženovienė, R., Tautvaišienė, G., Nordström, B., Stonkutė, E., & Barisevičius, G. 2015, Astronomy & Astrophysics, 576, A113
- Zhao, G., Mashonkina, L., Yan, H. L., et al. 2016, ApJ, 833, 225

TABLE 2
HYPATIA 2.1 UPDATE

Catalog	Telescope	Resolution ($\Delta\lambda/\lambda$)	S/N	λ Range (\AA)	Stellar Atmo	Eq. Width	CoG or SF	Solar Scale	Num. of FeI/II lines	Stars in Hypatia
Adibekyan et al. (2016)	HARPS (3.6 m ESO telescope, La Silla, Chile) and UVES (8m VLT / UT2 telescope, La Silla, Chile)		200-2300		ATLAS9 per Kurucz (1993)	ARES	MOOG per Sneden (1973)	Anders & Grevesse (1989)	250 / 40	39
Battistini & Bensh (2016)	FEROS on the ESO 1.5-m and 2.2-m telescopes and MIKE on the Magellan Clay telescope; UVES on the ESO Very Large Telescope	42000 - 65000	> 200	3500-9500	MARCS per (Gustafsson et al. 1975)	IRAF splot	Uppsala EQWIDTH	differential analysis	226 / 36	471
Baumann et al. (2010)	Robert G. Tull coude spectrograph on the 2.7 m Harlan Smith telescope; MIKE spectrograph on the 6.5 m Magellan Clay telescope; HARPS spectrograph on the 3.6 m ESO telescope	45000 - 110000	> 200	4500-7800 / 3350-9500 / 4445-8294	ATLAS9 per Kurucz (1993)	IRAF splot	MOOG per Sneden (1973)	differential analysis	34 / 11	117
Brewer et al. (2016)	HIRES spectrograph at the Keck I Telescope	70000	>200	5164-7800	ATLAS per Kurucz (1993)	spectral fitting	spectral fitting	differential analysis	600 / 300	894
Chen et al. (2001)	2.16m telescope at Beijing Astronomical Observatory (BAO) with the Coude Echelle Spectrograph (CES)	40000	>150	5500-9000	MARCS per (Gustafsson et al. 1975)	SPECTRUM	Uppsala EQWIDTH	Anders & Grevesse (1989)	142 / 8	143
da Silva et al. (2015)	Observatoire de Haute-Provence (OHP) using the ELODIE spectrograph	42000	> 200	3895-6815	ATLAS9 per Kurucz (1993)	ARES	MOOG per Sneden (1973)	differential analysis	72 / 12	304

* Telescope/spectrograph information and the techniques for determining abundances as given by the recently added literature sources (with more than 20 stars added) into *Hypatia* 2.1. Please see Hinkel et al. (2014, 2016) for more details. In the header, “S/N” is signal-to-noise report by the literature source, “ λ Range” is the wavelength coverage, “Stellar Atmo” is the stellar atmospheric model, “Eq. Width” is the package used to determine the equivalent width, “CoG or SF” designates whether the group used a curve-of-growth or spectral fitting technique where the package is specified in the former case, the “Solar Scale” is the solar normalization used by that group (differential analysis is cited where applicable), and “Num. of Fe I/II lines” lists the number of Fe I and Fe II lines.

TABLE 3
HYPATIA 2.1 UPDATE

Catalog	Telescope	Resolution ($\Delta\lambda/\lambda$)	S/N	λ Range (\AA)	Stellar Atmo	Eq. Width	CoG or SF	Solar Scale	Num. of Fe/II lines	Stars in Hypatia
Delgado Mena et al. (2014, 2015)	HARPS at 3.6-m ESO La Silla Observatory (Chile); UVES at 8.2-m Kueyen UT2 (VLT); FEROS at 2.2-m ESO/MPI telescope; SARG 3.5-m TNG; FIES at 2.6-m Nordic Optical Telescope; SOPHIE at 1.93-m OHP; CORALIE at 1.2-m Euler Swiss telescope; and UES at 4.2-m William Herschel Telescope	100000 / 115000 / 48000 / 57000- 86000 / 67000 / 75000 / 50000 / 55000	55% of the spectra > 200	3800-7000 / 3000-4800; 4800-6800 / 3600-9200 / 5100-10100 / 3700-7300 / 3820-6930 / 3800-6800 / 4600-7800	ATLAS9 per Kurucz (1993)	IRAF splot	MOOG2010 per Sneden (1973)	Anders & Grevesse (1989)	N/A	137 / 287
Gonzalez et al. (2001); Gonzalez et al. (2010); Gonzalez et al. (2010)	2.7m telescope at McDonald using the 2dcoude spectrometer and 4m Blanco Telescope at Cerro Tololo Inter-American Observatory (CTIO)	> 59000 / 35000	195-620	3700-10000 / 5850-8950	ATLAS9 per Kurucz (1993)	Uppsala EQWIDTH	MOOG per Sneden (1973)	their own	64 / 11	20 / 124
Gonzalez (2014, 2015)	McDonald Observatory 2.1-m Otto Struve telescope and Sandiford spectrograph	53000	300-350		ATLAS per Kurucz (1993)	DAOSPEC	MOOG per Sneden (1973)	differential analysis	45-55 / 6-8	37 / 30
Ghezzi et al. (2010)	FEROS on the MPG/ESO-2.20 m telescope	48000	> 200	3560-9200	ODFNEW / AT- LAS9 per Kurucz (1993)	ARES	MOOG per Sneden (1973)		27 / 12	149
Israelian et al. (2004, 2009)	4.2 m WHT/UES (La Palma); the 3.5 m TNG/SARG (La Palma); the 1.52 m ESO (La Silla) and the 1.2 m Swiss/CORALIE (La Silla)	55000 / 57000 / 50000 / 50000	150-350	3800-6800	ATLAS9 per Kurucz (1993) per Kurucz (1993)	IRAF splot	MOOG per Sneden (1973)	Anders & Grevesse (1989)	40 / 7	61 / 127
Lambert et al. (1991)	W. J. McDonald Observatory with the coude spectrographs of the 2.1-m and 2.7-m reflectors		> 150		ATLAS per Kurucz (1993)	Uppsala EQWIDTH	Uppsala EQWIDTH	Anders & Grevesse (1989)		61
Lambert & Reddy (2004)	2.7 m telescope at McDonald using the 2dcoude spectrometer	60000	100-200	3500-9000	ATLAS9 per Kurucz (1993)	IRAF splot	MOOG per Sneden (1973)	Reddy et al. (2003)	54 / 9	103
Liu et al. (2014)	High Dispersion Echelle Spectrograph at Okayama Astrophysical Observatory (OAO); which was equipped at the coude focus of the 1.88 m telescope	67000	> 200	5000-6200; 4000-7540	MAFAGS	spectral synthesis with IDL/Fortran SIU soft- ware (Reetz 1991)	spectral fitting	differential analysis		83
López-Valdivia et al. (2017)	2.1-m telescope of the Observatorio Astrofísico Guillermo Haro, located in Mexico, using the Cananea High-resolution Spectrograph (CanHiS)	80000	100	centered at 5005, 5890, 6310 and 6710 \AA	ATLAS12 per Kurucz (1993)	their own analysis	MOOG per Sneden (1973)	their own off Vesta	18 / 0	22

TABLE 4
HYPATIA 2.1 UPDATE

Catalog	Telescope	Resolution ($\Delta\lambda/\lambda$)	S/N	λ Range (\AA)	Stellar Atmo	Eq. Width	CoG or SF	Solar Scale	Num. of FeI/II lines	Stars in Hypatia
Luck & Heiter (2006)	2.1m telescope at McDonald using the CASPEC	60000	> 150	4840-7000	MARCS per (Gustafsson et al. 1975)75	spectral fitting	spectral fitting	differential analysis	450 / 25	194
Luck & Heiter (2007)	2.1m telescope at McDonald using the CASPEC	60000	> 150	4840-7000	MARCS per (Gustafsson et al. 1975)	LINES	MOOG per Sneden (1973)	differential analysis	332 / 18	296
Luck (2015, 2017)	McDonald Observatory using the 2.1m Struve Telescope and the Sandiford Cassegrain Echelle Spectrograph	60000	> 150	4840-7000	MARCS per (Gustafsson et al. 1975)	LINES	MOOG per Sneden (1973)	differential analysis	500 / 30-50	904 / 967
Mahdi et al. (2016)	ELODIE was on the 1.93 m telescope at Observatoire de Haute- Provence (OHP)	42000	> 70	4000-6800	MARCS per (Gustafsson et al. 1975)	iSpec per Blanco-Cuadros et al. (2014)	iSpec per Blacot & Gharasma (2014)	differential analysis	189	
Maldonado et al. (2015); Maldonado & Villaseca (2016)	HERMES spectrograph at the MERCATOR (1.2 m) telescope at La Palma observatory and FIES at the Nordic Optical Telescope (2.56 m)	85000 / 67000	90-340 / 75-480	3800-9000 / 3640-7360	ATLAS9 per Kurucz (1993)	WIDTH9 per (Kurucz 1993)	WIDTH9 per (Kurucz 1993)	differential analysis)	263 / 36	251 / 142
Mallik et al. (2003)	coude echelle spectrograph at the 102 cm telescope at the Vainu Bappu Observatory at Kavalur				MARCS per (Gustafsson et al. 1975)		MOOG per Sneden (1973)	differential analysis		71
Mishenina et al. (2012)	1.93m telescope at OHP using ELODIE	42000	100-350	3850-6800	ATLAS9 per Kurucz (1993)	WIDTH9 per (Kurucz 1993)	N/A	differential analysis	N/A	59
Mishenina et al. (2016)	1.93m telescope at OHP using ELODIE	42000	100-350	4400-6800	ATLAS9 per Kurucz (1993)	WIDTH9 per (Kurucz 1993)	N/A	differential analysis	N/A	196
Nissen (2013)	HARPS at 3.6-m ESO La Silla Observatory (Chile); FEROS at 2.2-m ESO/MPI telescope	115000 / 48000	250-1000 / 200-300	3800-6900 / 3500-9200	MARCS per (Gustafsson et al. 1975)	IRAF splot	Uppsala EQWIDTH	differential analysis	N/A	33
Nissen (2016)	HARPS (3.6 m ESO telescope, La Silla, Chile)	115000	>600	3800-6900	MARCS per (Gustafsson et al. 1975)	IRAF splot	Uppsala EQWIDTH	differential analysis	47 / 9	
Notsu et al. (2017)	High Dispersion Echelle Spectrograph attached at the 1.88-m reflector of Okayama Astrophysical Observatory (OAO)	59000		5600-9100 and 4300-7700	ATLAS9 per Kurucz (1993)	WIDTH9 per (Kurucz 1993)	SPSHOW (in the SPTOOL software developed by Y. Takeda; unpublished)	Anders & Grevesse (1989)	460 / 20	36
Pagano et al. (2017)	Magellan Inamori Kyocera Echelle (MIKE) spectrograph on the 6.5 meter Magellan II telescope	50000	150-300	4700-7100	ATLAS9 per Kurucz (1993)	ARES/IRAFMOOG14 per SPLOT	Sneden (1973)	Asplund et al. (2009)	69 / 14	508

TABLE 5
HYPATIA 2.1 UPDATE

Catalog	Telescope	Resolution ($\Delta\lambda/\lambda$)	S/N	λ Range (\AA)	Stellar Atmo	Eq. Width	CoG or SF	Solar Scale	Num. of FeI/II lines	Stars in Hypatia
Ramírez et al. (2013)	TS2/McD (R. G. Tull Coude spectrograph; 2.7 m Telescope at McDonald Observatory); HRS/HET (High Resolution Spectrograph; 9.2 m Hobby-Eberly Telescope); UVES/VLT (UV-Visual Echelle Spectrograph; 8 m Very Large Telescope); and FEROS/ESO (Fiber-fed Extended Range Optical Spectrograph; ESO 1.52-m Telescope)	60000 / 120000 / 80000 / 45000	> 100		MARCS per (Gustafsson et al. 1975)	IRAF splot	MOOG per Sneden (1973)	differential analysis		794
Suárez-Andrés et al. (2016)	3.6m telescope at ESO equipped with High Accuracy Radial Velocity Planet Searcher (HARPS) using CORALIE	110000	70-2000	3800-6900	ATLAS9 per Kurucz (1993)	ARES	MOOG per Sneden (1973)	Anders & Grevesse (1989)	263 / 36	1077
Takeda & Kawano (2005); Takeda et al. (2010)	1.8m telescope at Okayama Astrophysical Observatory (OAO) using the High Dispersion Echelle Spectrograph (HIDES)	70000	200	5800-7000	ATLAS9 per Kurucz (1993)	WIDTH9 per (Kurucz 1993)	SPSHOW (in the SPTOOL software developed by Y. Takeda; unpublished)	Anders & Grevesse (1989)	160 / 20	93 / 83
Trevisan & Barbuș (2014)	1.52m telescope at ESO using FEROS	48000	100	3560-9200	MARCS per (Gustafsson et al. 1975)	ARES	ABON2 via Spite 1967 (and improvements in the last 30yrs)	Trevisan et al. (2011)	97 / 9	65
Tucci Maia et al. (2016)	Magellan Inamori Kyocera Echelle (MIKE) spectrograph (Bernstein et al. 2003) on the 6.5m Clay Magellan Telescope at Las Campanas Observatory	>65000	400	3200-10000	MARCS per (Gustafsson et al. 1975)	IRAF splot	MOOG14 per Sneden (1973)	differential analysis	91 / 19	
Yan et al. (2016)	FOCES echelle spectrograph on the 2.2 m telescope at Calar Alto Observatory	> 40000	> 100	3700-9800	MAFAGS	spectral fitting	spectral fitting	Cu = 4.25; Fe = 7.51	0 / 8	32
Ženovienė et al. (2015)	Fibre-fed Echelle Spectrograph (FIES) on the Nordic Optical 2.5 m telescope	68000	> 100	3680-7270	MARCS per (Gustafsson et al. 1975)	spectral fitting (EQWIDTH)	spectral fitting (BSYN)	differential analysis	N/A	44
Zhao et al. (2016)	1.52m telescope at ESO using FEROS	48000	100	3560-9200	MARCS per (Gustafsson et al. 1975)	ARES	ABON2 via Spite 1967 (and improvements in the last 30yrs)	Anders & Grevesse (1989)	97 / 9	35

CATSUP for FGK-Stars Within 30 pc

* Telescope/spectrograph information and the techniques for determining abundances as given by the recently added literature sources (with more than 20 stars added) into *Hypatia* 2.1. Please see Hinkel et al. (2014, 2016) for more details. In the header, “S/N” is signal-to-noise report by the literature source, “ λ Range” is the wavelength coverage, “Stellar Atmo” is the stellar atmospheric model, “Eq. Width” is the package used to determine the equivalent width, “CoG or SF” designates whether the group used a curve-of-growth or spectral fitting technique where the package is specified in the former case, the “Solar Scale” is the solar normalization used by that group (differential analysis is cited where applicable), and “Num. of Fe I/II lines” lists the number of Fe I and Fe II lines.

TABLE 6
PARAMETERS IN CATSUP

Column Header	Description
HIP	Hipparcos name
HD	Henry-Draper catalog name
TYC	TYCHO name
RAJ2000	Right ascension (epoch = 2000)
DEJ2000	Declination (epoch = 2000)
X	geocentric x-coordinate from the Sun, in pc
Y	geocentric y-coordinate from the Sun, in pc
Z	geocentric z-coordinate from the Sun, in pc
Uvel	velocity (km/s) positive toward the Galactic anticenter (radial)
Vvel	velocity (km/s) positive in the direction of Galactic rotation
Wvel	velocity (km/s) positive toward the North Galactic Pole
Dist	distance in pc (from Gaia)
Teff	effective temperature of the star, in K
TeffSrc	effective temperature reference source, namely PASTEL (Soubiran et al. 2016, and references therein), ExoCat (Gray et al. 2003, 2006; Valenti & Fischer 2005; Takeda et al. 2007, and V-K data, see paper)
logg	surface gravity of the star
loggSrc	surface gravity reference source, namely PASTEL (Soubiran et al. 2016, and references therein), ExoCat (Gray et al. 2003, 2006; Valenti & Fischer 2005; Takeda et al. 2007, and V-K data, see paper)
Disk	likely origin within the disk (thin, thick, N/A) based on kinematics
Planet	flag (0, 1) as to whether a planet is known to orbit the star at the time of this publication, based on the NASA Exoplanet Archive
Bmag	B magnitude
Vmag	V magnitude
BV	B-V color
Single	a true single star (=1)
Component	if known to be a member of a multiple, to which component the HIP number is referring (A, B, etc.). If the HIP number includes more than one star, either a known or suspected unresolved/very faint companion, noted by a “+” symbol
HIP2	if more than one star in the system has its own HIP number, the other associated HIP numbers
SpType	spectral type
SpecSrc	spectral type reference source, where the ADS suffix is provided in all cases. An asterisk (*) at the end of the reference indicates that the Houk spectral type was adjusted to modern MK system (using Gray et al. 2003, 2006 spectral types) following Pecaat & Mamajek (2016).
logRHK	the average value of $\log R'_{HK}$ Ca II HK emission indices derived from literature sources
logRHKsources	number of sources compiled for the $\log R'_{HK}$ Ca II HK emission indices
FeH	[Fe/H] abundance in dex
spFeH	spread in [Fe/H] abundance
CH	[C/H] abundance in dex
spCH	spread in [C/H] abundance
OH	[O/H] abundance in dex
spOH	spread in [O/H] abundance
NaH	[Na/H] abundance in dex
spNaH	spread in [Na/H] abundance
MgH	[Mg/H] abundance in dex
spMgH	spread in [Mg/H] abundance
AlH	[Al/H] abundance in dex
spAlH	spread in [Al/H] abundance
SiH	[Si/H] abundance in dex
spSiH	spread in [Si/H] abundance
CaH	[Ca/H] abundance in dex
spCaH	spread in [Ca/H] abundance
TiH	[Ti/H] abundance in dex
spTiH	spread in [Ti/H] abundance
VH	[V/H] abundance in dex
spVH	spread in [V/H] abundance
CrH	[Cr/H] abundance in dex
spCrH	spread in [Cr/H] abundance
MnH	[Mn/H] abundance in dex

TABLE 6 — *Continued*

Column Header	Description
spMnH	spread in [Mn/H] abundance
CoH	[Co/H] abundance in dex
spCoH	spread in [Co/H] abundance
NiH	[Ni/H] abundance in dex
spNiH	spread in [Ni/H] abundance
FUVmag	FUV magnitude (AB mag)
FUVmagerr	error in FUV magnitude (AB mag)
NUVmag	NUV magnitude (AB mag)
NUVmagerr	error in NUV magnitude (AB mag)
l_limit	lower limit flag for FUV flux
FUVflux	FUV flux (μJy)
FUVfluxerr	error in FUV flux (μJy)
u_limit	upper limit flag for NUV flux
NUVflux	NUV flux (μJy)
NUVfluxerr	error in NUV flux (μJy)
logRx	$\log R_x$, where $R_x = L_x/L_{bol}$, X-ray to bolometric luminosity ratio or the fractional X-ray luminosity
logLLsun	$\log(L/L_\odot)$, bolometric luminosity in Suns**
Lbol	L_{bol} , bolometric luminosity
fROSAT	\log_{10} of X-ray flux from ROSAT ($\text{erg s}^{-1} \text{cm}^{-2}$)
fsROSAT	\log_{10} of X-ray surface flux from ROSAT ($\text{erg s}^{-1} \text{cm}^{-2}$)
LROSAT	\log_{10} of X-ray luminosity from ROSAT (erg s^{-1})
RxROSAT	\log_{10} of $R_x (= L_x/L_{bol})$ from ROSAT
fXMM	\log_{10} of X-ray flux from XMM ($\text{erg s}^{-1} \text{cm}^{-2}$)
fsXMM	\log_{10} of X-ray surface flux from XMM ($\text{erg s}^{-1} \text{cm}^{-2}$)
LXMM	\log_{10} of X-ray luminosity from XMM (erg s^{-1})
RxXMM	\log_{10} of $R_x (= L_x/L_{bol})$ XMM
fChan	\log_{10} of X-ray flux from Chandra ($\text{erg s}^{-1} \text{cm}^{-2}$)
fsChan	\log_{10} of X-ray surface flux from Chandra ($\text{erg s}^{-1} \text{cm}^{-2}$)
LChan	\log_{10} of X-ray luminosity from Chandra (erg s^{-1})
RxChan	\log_{10} of $R_x (= L_x/L_{bol})$ from Chandra

* All values of 99.99 are null.

** in units of the IAU nominal solar luminosity: $L_{Sun} = 3.828 \times 10^{26}$ W (Prša et al. 2016)